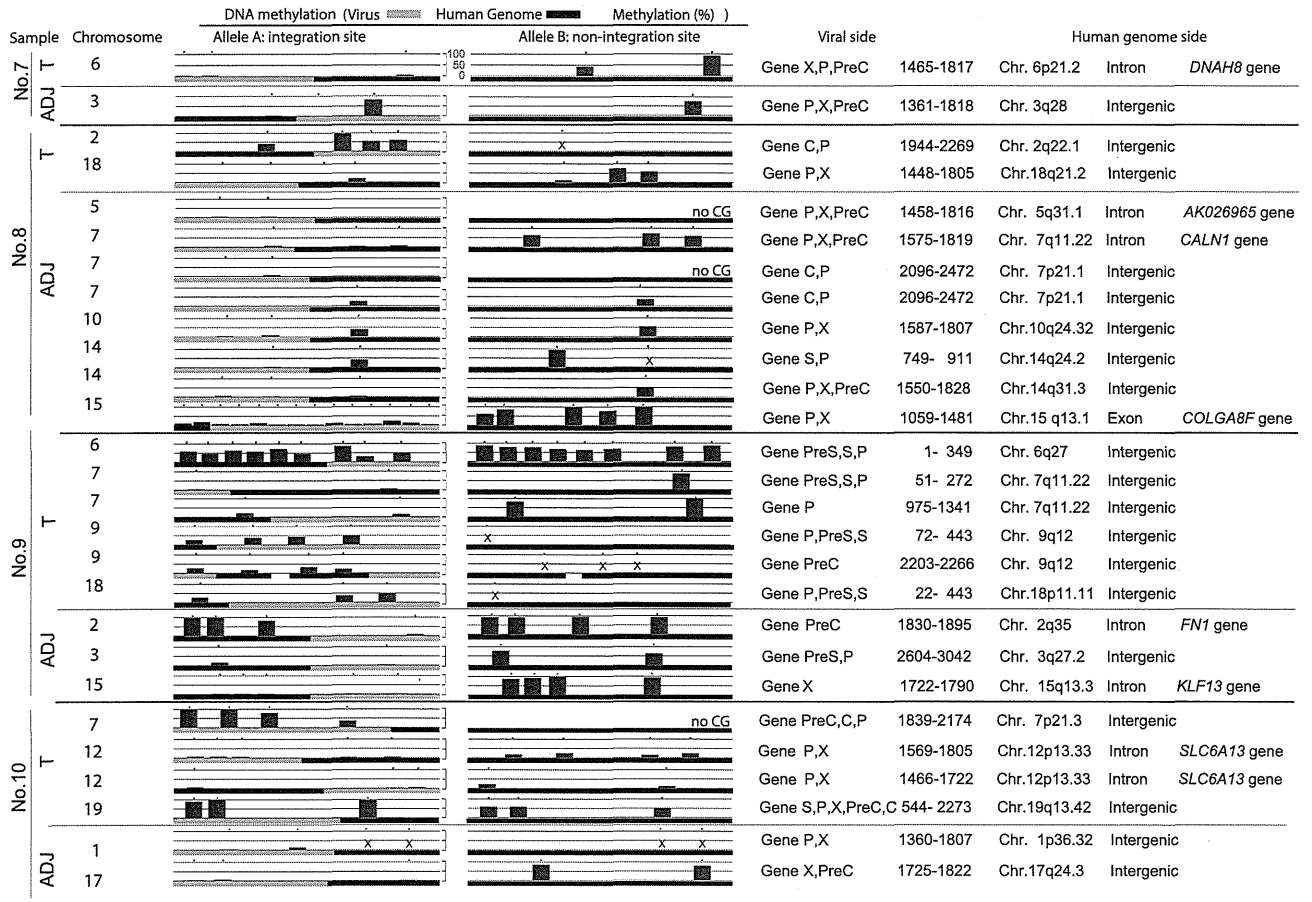

Sample		Chromosome	Viral side		Human genome side		
No.7	T	6	Gene X,P,PreC	1465-1817	Chr. 6p21.2	Intron	*DNAH8* gene
	ADJ	3	Gene P,X,PreC	1361-1818	Chr. 3q28	Intergenic	
No.8	T	2	Gene C,P	1944-2269	Chr. 2q22.1	Intergenic	
		18	Gene P,X	1448-1805	Chr.18q21.2	Intergenic	
	ADJ	5	Gene P,X,PreC	1458-1816	Chr. 5q31.1	Intron	*AK026965* gene
		7	Gene P,X,PreC	1575-1819	Chr. 7q11.22	Intron	*CALN1* gene
		7	Gene C,P	2096-2472	Chr. 7p21.1	Intergenic	
		7	Gene C,P	2096-2472	Chr. 7p21.1	Intergenic	
		10	Gene P,X	1587-1807	Chr.10q24.32	Intergenic	
		14	Gene S,P	749- 911	Chr.14q24.2	Intergenic	
		14	Gene P,X,PreC	1550-1828	Chr.14q31.3	Intergenic	
		15	Gene P,X	1059-1481	Chr.15 q13.1	Exon	*COLGA8F* gene
No.9	T	6	Gene PreS,S,P	1- 349	Chr. 6q27	Intergenic	
		7	Gene PreS,S,P	51- 272	Chr. 7q11.22	Intergenic	
		7	Gene P	975-1341	Chr. 7q11.22	Intergenic	
		9	Gene P,PreS,S	72- 443	Chr. 9q12	Intergenic	
		9	Gene PreC	2203-2266	Chr. 9q12	Intergenic	
		18	Gene P,PreS,S	22- 443	Chr.18p11.11	Intergenic	
	ADJ	2	Gene PreC	1830-1895	Chr. 2q35	Intron	*FN1* gene
		3	Gene PreS,P	2604-3042	Chr. 3q27.2	Intergenic	
		15	Gene X	1722-1790	Chr. 15q13.3	Intron	*KLF13* gene
No.10	T	7	Gene PreC,C,P	1839-2174	Chr. 7p21.3	Intergenic	
		12	Gene P,X	1569-1805	Chr.12p13.33	Intron	*SLC6A13* gene
		12	Gene P,X	1466-1722	Chr.12p13.33	Intron	*SLC6A13* gene
		19	Gene S,P,X,PreC,C	544- 2273	Chr.19q13.42	Intergenic	
	ADJ	1	Gene P,X	1360-1807	Chr. 1p36.32	Intergenic	
		17	Gene X,PreC	1725-1822	Chr.17q24.3	Intergenic	

Figure 4. Allele-specific methylation analysis of the tumor (*T*) and adjacent nontumor (ADJ) sample genomes. The methylation levels of the HBV and human genomes for the integrated and unintegrated alleles in four paired tumor and adjacent nontumor samples (sample nos. 7–10) are shown. Detailed results of the HBV integrants (*PreC, Precore; C, Core; PreS, Presurface; S, Surface; X, X*) and flanking host genomes (position, chromosome, location of the genome, and gene names) are shown. The HBV genome became significantly methylated when integrated into highly methylated human genome regions, but not when integrated into unmethylated human genome regions. (×) The desired quantitative methylation levels were not obtained because of technical difficulties with the sequences that were being analyzed.

The dynamic changes in DNA methylation described here have a major functional impact on the biological behavior of HBV and underlie the molecular mechanisms that control infection or enable tumorigenesis. These findings may significantly impact public health given that millions of people worldwide are carriers of HBV. Distinct DNA methylation profiles may exist, for example, between primary HCCs in Japanese patients and those of other nationalities. Additional studies are needed to address this issue, and research into the influence of other environmental factors is required.

Increased viral DNA methylation is present in cancers associated with DNA viruses, including human papilloma virus types 16 and 18 (HPV 16 and 18) (Fernandez et al. 2009; Mirabello et al. 2012), Epstein-Barr virus (Uozaki and Fukayama 2008; Fernandez et al. 2009), and human T-lymphotropic virus 1 (Taniguchi et al. 2005). An analysis of the haplotype-resolved genome and epigenome of the aneuploid HeLa cervical cancer cell line revealed that an amplified, highly rearranged region of chromosome 8q24.21 harboring an integrated HPV18 genome likely represents the tumor-initiating event (Adey et al. 2013). Whether the dynamic changes in DNA methylation observed in cells with integrated HBV genomes also occur in human cells infected by other viruses is an interesting question for further study. We anticipate that our assay will be a powerful tool for this purpose and have successfully detected integrated HPV sequences in the genomes of cervical cancer cell lines (Y Watanabe, H Yamamoto, F Itoh, and N Suzuki, unpubl.).

This study provides novel mechanistic insights into HBV-mediated hepatocarcinogenesis, which may have preventive and therapeutic applications for carriers of HBV and patients with HBV-HCC, as it suggests that epigenetic alterations provide candidate biochemical markers and therapeutic targets. This study, together with a recent global survey of HBV integration events (Ding et al. 2012; Fujimoto et al. 2012; Jiang et al. 2012; Sung et al. 2012; Toh et al. 2013), provides a foundation for the further experimentation and mechanistic understanding of HBV-HCC.

Methods

Cell lines and primary tissues

The PLC/PRF/5 (Alexander) human hepatoma cell line was obtained from the Japanese Collection of Research Bioresources (JCRB). HepG2.2.15 cells, kindly gifted by Professor Stephan Urban

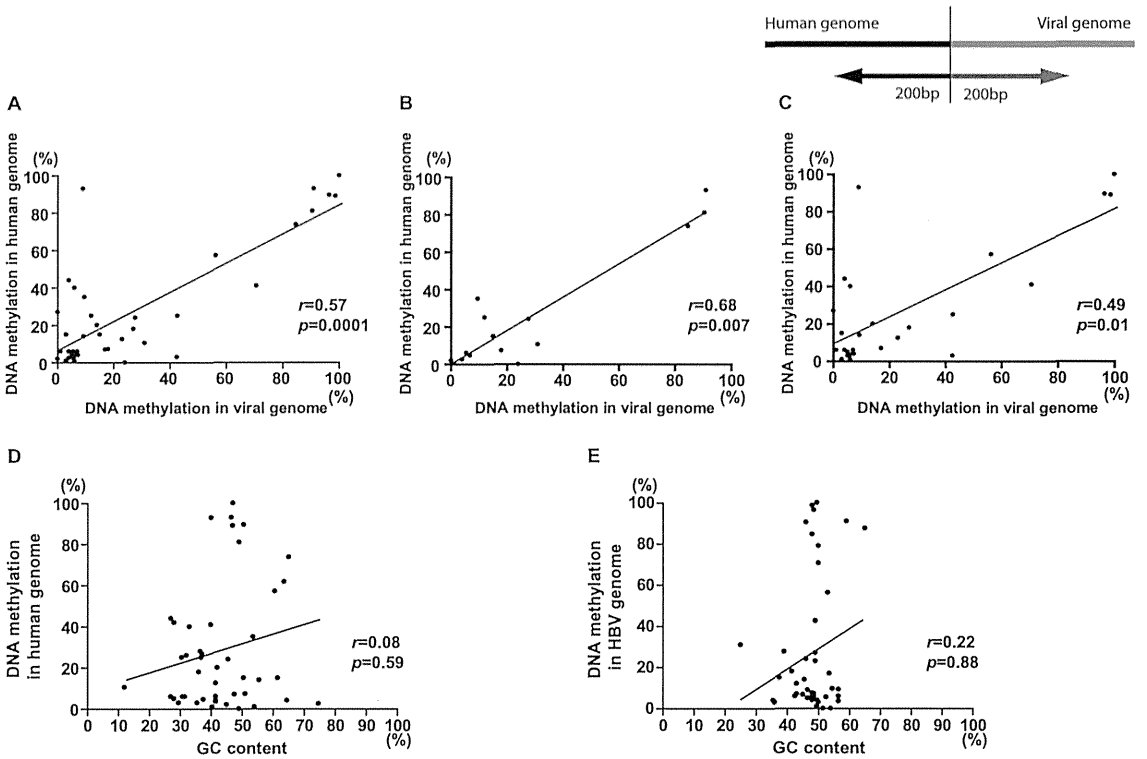

Figure 5. Correlation analysis between the methylation pattern of the integrated HBV DNA and that of the human genome. DNA fragments, including 200 bp of the HBV DNA and 200 bp of the human genome around the boundary, were analyzed for average methylation and GC content. (*A*) A correlation between the average methylation of the HBV DNA and that of the human genome in combined two cell lines and eight clinical samples ($n = 40$, $r = 0.57$, $P = 0.0001$, 95%CI = 0.3091–0.7545). (*B*) A correlation between the average methylation of the HBV DNA and that of the human genome in two cell lines ($n = 14$, $r = 068$, $P = 0.007$, 95%CI = 0.2233–0.8946). (*C*) A correlation between the average methylation of the HBV DNA and that of the human genome in eight clinical samples ($n = 26$, $r = 0.49$, $P = 0.01$, 95%CI = 0.1222–0.7463). (*D*) No correlation between the average methylation and GC contents in the human genome in the combined two cell lines and eight clinical samples ($n = 45$, $r = 0.08$, $P = 0.59$, 95%CI = −0.2253–0.3745). (*E*) No correlation between the average methylation and GC contents in the viral genome in the combined two cell lines and eight clinical samples ($n = 47$, $r = 0.22$, $P = 0.88$, 95%CI = −0.3151–0.2751).

at University Hospital Heidelberg, was derived from HepG2 cells transfected with a plasmid carrying four 5′-3′ tandem copies of the HBV genome (Koike et al. 1994). Cell lines were maintained in appropriate media containing 10% fetal bovine serum in plastic culture plates. Primary tissues from tumor and adjacent tissues were obtained at the time of the clinical procedures. Informed consent was obtained from all the patients before specimen collection. This study was approved by the institutional review board. DNA was extracted using the standard phenol–chloroform method. The concentration and quantity of extracted DNA were measured using a NanoDrop spectrophotometer (NanoDrop Technologies).

MCAM analysis

MCAM analysis was conducted as previously described (Oishi et al. 2012). A detailed protocol of MCA was previously described (Toyota et al. 1999). We used a custom human promoter array (G4426A-02212; Agilent Technologies) comprising 36,579 probes corresponding to 9021 unique genes. The probes on the array were selected to recognize SmaI/XmaI fragments mainly derived from sequences near gene transcription start sites. Five micrograms of genomic DNA was digested with 100 U of methylation-sensitive restriction endonuclease SmaI (New England Biolabs) for 24 h at 25°C, which cleaves unmethylated DNA leaving blunt ends (CCC/GGG). Subsequently, the DNA was digested with 20 U of methylation-insensitive restriction endonuclease XmaI for 6 h at 37°C, creating sticky ends (C/CCGGG). Five hundred milligrams of digested DNA was ligated using 50 μL of RMCA12 (5′-CCGGGCA GAAAG-3′)/RMCA24 (5′-CCACCGCCATCCGAGCCTTTCTGC-3′) primers and T4 DNA ligase (TaKaRa Bio) for 16 h at 16°C. After filling in the overhanging ends of the ligated DNA fragments at 72°C, the DNA was amplified for 5 min at 95°C followed by 25 cycles of 1-min incubation at 95°C and 3-min incubation at 77°C using 100 pmol of RMCA24 primer. MCA products were labeled with Cy5 (red) for DNA from hepatoma samples (both tumor and adjacent normal) and Cy3 (green) for DNA from human blood mixture of three healthy volunteers using a randomly primed Klenow polymerase reaction (Invitrogen) for 3 h at 37°C. Human CpG island arrays (4 × 44 K) were purchased from Agilent Technologies. Microarray protocols, including labeling, hybridization, and post-hybridization washing procedures, are provided at http://www.agilent.com/. Labeled samples were then hybridized to arrays in the presence of human Cot-1 DNA for 24 h at 65°C. After washing, arrays were scanned using an Agilent DNA microarray scanner and analyzed using Agilent Feature Extraction software (FE version 9.5.1.1, Agilent Technologies) at St. Marianna University School of Medicine. We used GeneSpring software (Agilent) for choosing candidate genes after normalization of the raw data.

DNA methylation analysis

Hidden Markov models have been successfully used to partition genomes into segments of comparable stochastic structure (Durbin et al. 1998). Using these models for sequence analysis performed

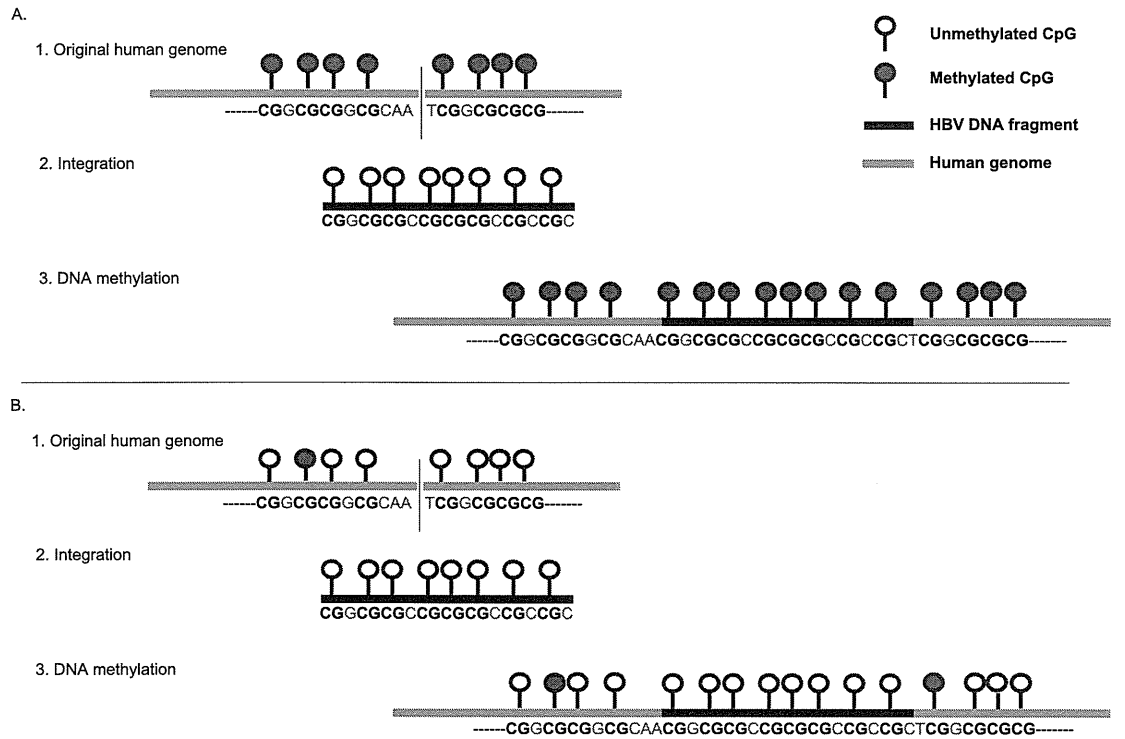

Figure 6. Schema of DNA methylation at HBV integrants and flanking human genomic sequences. (*A*) DNA hypermethylation was seen in both the integrated HBV fragment and human genome (original human genome shows dense methylation). The HBV genome often showed significant methylation when integrated into highly methylated host sites. (*B*) DNA hypermethylation was rarely seen in the integrated HBV fragment and human genome (original human genome shows low methylation). The HBV genome remained largely unmethylated when integrated into unmethylated host sites.

on the CpG plugin of bioinformatics software Geneious 5.5.8 (Biomatters), CpG islands were searched in the HBV genome (Kearse et al. 2012). Bisulfite PCR was performed using an EpiTect Bisulfite Kit (Qiagen) according to the manufacturer's protocol. One microliter of bisulfite-treated DNA was used as a template. The primers used for amplifying CpG sequences in the *HBx* gene are described in Supplemental Table 1. After PCR, the biotinylated strand was captured on streptavidin-coated beads (Amersham Bioscience) and incubated with sequencing primers (Supplemental Table 1). The pyrosequencing reactions were performed using the PyroMark Q24 and/or PyroMark Q24 advanced (Qiagen). Pyrosequencing quantitatively measures the methylation status of several CpG sites in a given sequence. These adjacent sites usually show highly concordant methylation. Therefore, the mean percentage of methylation at detected sites was used as a representative value for each sequence.

LINE1 and *Alu*Yb8 methylation analysis

The LINE1 and *Alu*Yb8 methylation levels, as measured by pyrosequencing, are good indicators of the cellular levels of 5-methylcytosine (i.e., the global DNA methylation level). To quantify relatively high LINE1 and *Alu*Yb8 methylation levels, we used pyrosequencing technology (Igarashi et al. 2010). PCR and subsequent pyrosequencing for LINE1 and *Alu*Yb8 were performed using the PyroMark kit (Qiagen). This assay amplifies a region of the LINE1 or *Alu*Yb8 elements that includes three CpG sites. The PCR was conducted as follows: 45 cycles for 20 sec at 95°C, for 20 sec at 50°C, and for 20 sec at 72°C, followed by 5 min at 72°C. The biotinylated PCR product was purified and converted to single strands to serve as a template for the pyrosequencing reaction using the pyrosequencing vacuum prep tool (Qiagen). The pyrosequencing reactions were performed using the PyroMark Q24 and/or PyroMark Q24 advanced (Qiagen). The percentage of Cs relative to the total sum of the Cs and Ts at each CpG site was calculated. The average of the percentages of Cs at the three CpG sites was used to represent the overall LINE1 and *Alu*Yb8 methylation levels in each sample.

FISH analysis of HBV integration

We developed a FISH analysis method to detect HBV DNA and demonstrate its presence in PLC/PRF/5 cells (Supplemental Fig. 3). The slides were pretreated with hydrogen peroxide and rinsed in 1× phosphate-buffered saline (PBS) to minimize background and quench endogenous peroxidase activity. To remove the excess cytoplasm, the slides were treated with pepsin and then fixed with 1% formaldehyde in PBS/$MgCl_2$. The slides were then dehydrated in an ethanol series (70%, 90%, and 100%) for 3 min at each step. The probes were designed based on the reference HBV sequence in PLC/PRF/5 DNA that is available from the Methylyzer 1.0 website (http://gbrowse.bioinfo.cnio.es/cgi-bin/VIRUS/HBV/). The FISH probes were prepared by combining the PCR-labeled probes (Supplemental Table 1), human Cot-1 DNA, and salmon sperm DNA. The probes were precipitated and mixed with hybridization buffer, and the probe DNA cocktail was denatured for 5 min at 95°C. The DNA on the slides was denatured by soaking in 70% formamide/2× SSC for 3 min at 74°C. The slides were immediately immersed in freshly prepared ice-cold 70% ethanol for 3 min, followed by 3-min immersions in 90% and then 100% ethanol. The denatured probe DNA was applied to the dry denatured slides and covered with a coverslip. The hybridization was performed for 16 h at 37°C.

Tyramide signal amplification (TSA)–FISH

TSA (tyramide signal amplification) detection kits were obtained from PerkinElmer. TSA-FISH detection was performed following the manufacturer's protocols with minor modifications. High stringency washes (0.1× SSC) were used to reduce the background, and TNT buffer (0.1 M Tris-HCl at pH 7.5, 0.15 M NaCl, 0.05% Tween 20) was adjusted to pH 7.0–7.5. The biotin- or DIG-labeled probes were detected using streptavidin-HRP or anti-DIG-HRP in TNB (0.1 M Tris-HCl at pH 7.5, 0.15 M NaCl, 0.05% blocking reagent [supplied in the kit]) for 30 min at room temperature and washed twice for 5 min each in TNT buffer. For the tyramide amplification procedure, the slide was covered with tyramide solution (Tyr-Bio, 1:50) for 10 min at room temperature. The tyramide solution was removed, and the slides were washed twice for 5 min each with TNT at room temperature. Fluorochrome-conjugated streptavidin (stAv-Alexa 488) diluted in TNB was used to detect the Tyr-Bio. The slides were incubated for 30 min at room temperature, washed with TNT buffer twice for 5 min each at room temperature, and covered with an anti-fade reagent containing DAPI (Speel et al. 1997; Schriml et al. 1999).

Identification of the chromosomal locations of viral–host junctions

The viral–host junctions were amplified using primers specific for human *Alu*Yb8 repetitive sequences and HBV X regions (Supplemental Table 1; Minami et al. 1995; Murakami et al. 2004). One microliter of genomic DNA solution served as a template in the subsequent PCR. We used touchdown PCR for most of the assays. All PCR assays included a denaturation step for 30 sec at 95°C, followed by an annealing step at various temperatures for 30 sec and an extension step for 30 sec at 72°C. PCR products were analyzed using electrophoresis through 1% agarose gels. PCR products were ligated to pCR-XL-TOPO vector DNA (TOPO XL PCR Cloning kit; Invitrogen) and transformed into competent cells. Positive colonies were selected and isolated using a QIA prep Spin Miniprep Kit (Qiagen). Direct sequence analysis of TOPO-TA cloning products was performed using a 3130 genetic analyzer (Applied Biosystems) (Watanabe et al. 2011). All sequences were searched for matches with HBV and pCR-XL-TOPO sequences using Geneious 5.5.8 (Biomatters) sequence analysis and assembly software and the BLAST program available on the UCSC Genome Browser (http://genome.ucsc.edu/).

Analysis of HBV DNA integration site sequences using NGS

Agilent's SureSelect target enrichment system is a highly efficient hybrid selection technique for optimizing NGS. We used this system and 12,391 custom baits covering the DNA sequences of HBV genotypes A to J and PLC/PRF/5 HBV sequences and optimized experiments for a GS FLX Titanium system (Roche). PLC/PRF/5, HepG2.2.15, and four paired tumor and nontumor samples (sample nos. 7, 8, 9, and 10 in Fig. 1B) were analyzed.

DNA methylation analysis of the integrated HBV genome as well as the adjacent human genome

DNA methylation was analyzed using bisulfite pyrosequencing (Oishi et al. 2012). The pyrosequencing reactions were performed using the PyroMark Q24 and/or PyroMark Q24 advanced (Qiagen). PLC/PRF/5, HepG2.2.15, and four paired tumor and nontumor samples (sample nos. 7, 8, 9, and 10 in Fig. 1B) were analyzed. Primers for methylation analysis of integration sites in PLC/PRF/5 are shown in Supplemental Table 1.

DNA methylation analysis of orthologous loci

Methylation levels of orthologous loci in HepG2.2.15 cells and in PBLs of a healthy volunteer at the same (empty) target sites of PLC/PRF/5 cells were analyzed using bisulfite pyrosequencing. Similarly, methylation levels of orthologous loci in PLC/PRF/5 cells and in PBLs at the same (empty) target sites of HepG2.2.15 cells were analyzed.

Allele-specific DNA methylation analysis of the integrated HBV genome as well as the adjacent human genome

Allele-specific DNA methylation was analyzed as described previously (Yamada and Ito 2011). The pyrosequencing reactions were performed using the PyroMark Q24 and/or PyroMark Q24 advanced (Qiagen).

Correlation analysis between the methylation pattern of the integrated HBV DNA and that of the human genome

DNA fragments, including 200 bp of the integrated HBV DNA and 200 bp of the human genome around the boundary, were analyzed for average methylation, GC content, and repetitive sequences in cell lines and clinical samples. RepeatMasker was used to identify repetitive elements in genomic sequences (AFA Smit, R Hubley, P Green, unpubl.). The Spearman correlation coefficient was used to assess correlations between the average methylation of the HBV DNA and that of the human genome. Correlations between GC content or repetitive sequences in the HBV DNA and the human genome were analyzed by using the Spearman correlation coefficient for continuous variables, and $P < 0.05$ was considered significant. All statistical analyses were performed using PRISM software for Windows, version 4 (GraphPad Prism).

Chromatin structure at the integrated HBV site

Using Bander software (Cheung et al. 2001; Furey and Haussler 2003), we analyzed the chromatin structure at the integrated HBV site in PLC/PRF/5 and HepG2.2.15.

Data access

All raw sequence data from this study have been submitted to the DDBJ Japanese Genotype-phenotype Archive (JGA; http://trace.ddbj.nig.ac.jp/jga/index_e.html) under accession number JGAS00000000015. Array data have been submitted to the NCBI Gene Expression Omnibus (GEO; http://www.ncbi.nlm.nih.gov/geo/) under accession number GSE59405.

Acknowledgments

We thank Drs. K. Watashi and T. Wakita for cell lines and Drs. T. Takayama, K. Takasaki, and S. Kawasaki for clinical samples. We also thank Drs. N. Matsumoto and N. Yamada-Ohkawa, as well as other members of the laboratory, for advice and suggestions. A part of the data used for this research was originally obtained by a research project of Hiroyuki Yamamoto and Yoshiyuki Watanabe led by Professor Fumio Itoh and is available at the website of the NBDC/JST (http://biosciencedbc.jp/en/). This work was supported in part by the Japan Society for the Promotion of Science (JSPS) Grants-in-Aid for Scientific Research (JSPS KAKENHI grant no. 23590964 to H. Yotsuyanagi).

Author contributions: Y.W. conceived the study, designed and performed the experiments, analyzed the data, and wrote the manuscript. H. Yamamoto designed the experiments, analyzed the data and wrote the manuscript. R.O. performed the experiments

and analyzed the data. M.T. provided intellectual support. M.Y., N.K., S.T., and A.S. provided clinical samples. H. Yotsuyanagi designed the experiments, analyzed the data and wrote the manuscript. K.K. provided intellectual support. F.I. supervised all aspects of the study.

References

Adey A, Burton JN, Kitzman JO, Hiatt JB, Lewis AP, Martin BK, Qiu R, Lee C, Shendure J. 2013. The haplotype-resolved genome and epigenome of the aneuploid HeLa cancer cell line. *Nature* **500:** 207–211.

Burgers WA, Blanchon L, Pradhan S, de Launoit Y, Kouzarides T, Fuks F. 2007. Viral oncoproteins target the DNA methyltransferases. *Oncogene* **26:** 1650–1655.

Cheung VG, Nowak N, Jang W, Kirsch IR, Zhao S, Chen XN, Furey TS, Kim UJ, Kuo WL, Olivier M, et al. 2001. Integration of cytogenetic landmarks into the draft sequence of the human genome. *Nature* **409:** 953–958.

Ding D, Lou X, Hua D, Yu W, Li L, Wang J, Gao F, Zhao N, Ren G, Li L, et al. 2012. Recurrent targeted genes of hepatitis B virus in the liver cancer genomes identified by a next-generation sequencing-based approach. *PLoS Genet* **8:** e1003065.

Doerfler W. 2008. In pursuit of the first recognized epigenetic signal-DNA methylation: a 1976 to 2008 synopsis. *Epigenetics* **3:** 125–133.

Doerfler W, Remus R, Müller K, Heller H, Hohlweg U, Schubbert R. 2001. The fate of foreign DNA in mammalian cells and organisms. *Dev Biol* **106:** 89–97.

Durbin R, Eddy S, Krogh A, Mitchison G. 1998. *Biological sequence analysis*. Cambridge University Press, Cambridge, UK.

Fernandez AF, Rosales C, Lopez-Nieva P, Graña O, Ballestar E, Ropero S, Espada J, Melo SA, Lujambio A, Fraga MF, et al. 2009. The dynamic DNA methylomes of double-stranded DNA viruses associated with human cancer. *Genome Res* **19:** 438–451.

Fujimoto A, Totoki Y, Abe T, Boroevich KA, Hosoda F, Nguyen HH, Aoki M, Hosono N, Kubo M, Miya F, et al. 2012. Whole-genome sequencing of liver cancers identifies etiological influences on mutation patterns and recurrent mutations in chromatin regulators. *Nat Genet* **44:** 760–764.

Furey TS, Haussler D. 2003. Integration of the cytogenetic map with the draft human genome sequence. *Hum Mol Genet* **12:** 1037–1044.

Gatza ML, Chandhasin C, Ducu RI, Marriott SJ. 2005. Impact of transforming viruses on cellular mutagenesis, genome stability, and cellular transformation. *Environ Mol Mutagen* **45:** 304–325.

Hilleman MR. 2004. Strategies and mechanisms for host and pathogen survival in acute and persistent viral infections. *Proc Natl Acad Sci* **101:** 14560–14566.

Igarashi S, Suzuki H, Niinuma T, Shimizu H, Nojima M, Iwaki H, Nobuoka T, Nishida T, Miyazaki Y, Takamaru H, et al. 2010. A novel correlation between LINE-1 hypomethylation and the malignancy of gastrointestinal stromal tumors. *Clin Cancer Res* **16:** 5114–5123.

Jiang Z, Jhunjhunwala S, Liu J, Haverty PM, Kennemer MI, Guan Y, Lee W, Carnevali P, Stinson J, Johnson S, et al. 2012. The effects of hepatitis B virus integration into the genomes of hepatocellular carcinoma patients. *Genome Res* **22:** 593–601.

Kan Z, Zheng H, Liu X, Li S, Barber TD, Gong Z, Gao H, Hao K, Willard MD, Xu J, et al. 2013. Whole-genome sequencing identifies recurrent mutations in hepatocellular carcinoma. *Genome Res* **23:** 1422–1433.

Kearse M, Moir R, Wilson A, Stones-Havas S, Cheung M, Sturrock S, Buxton S, Cooper A, Markowitz S, Duran C, et al. 2012. Geneious Basic: an integrated and extendable desktop software platform for the organization and analysis of sequence data. *Bioinformatics* **28:** 1647–1649.

Kim CM, Koike K, Saito I, Miyamura T, Jay DG. 1991. HBx gene of hepatitis B virus induces liver cancer in transgenic mice. *Nature* **351:** 317–320.

Koike K, Moriya K, Iino S, Yotsuyanagi H, Endo Y, Miyamura T, Kurokawa K. 1994. High-level expression of hepatitis B virus HBx gene and hepatocarcinogenesis in transgenic mice. *Hepatology* **19:** 810–819.

Lau C-C, Sun T, Ching AK, He M, Li JW, Wong AM, Co NN, Chan AW, Li PS, Lung RW, et al. 2014. Viral-human chimeric transcript predisposes risk to liver cancer development and progression. *Cancer Cell* **25:** 335–349.

Li S, Mao M. 2013. Next generation sequencing reveals genetic landscape of hepatocellular carcinomas. *Cancer Lett* **340:** 247–253.

Lupberger J, Hildt E. 2007. Hepatitis B virus–induced oncogenesis. *World J Gastroenterol* **13:** 74–81.

Minami M, Poussin K, Brechot C, Paterlini P. 1995. A novel PCR technique using *Alu*-specific primers to identify unknown flanking sequences from the human genome. *Genomics* **29:** 403–408.

Mirabello L, Sun C, Ghosh A, Rodriguez AC, Schiffman M, Wentzensen N, Hildesheim A, Herrero R, Wacholder S, Lorincz A, et al. 2012. Methylation of human papillomavirus type 16 genome and risk of cervical precancer in a Costa Rican population. *J Natl Cancer Inst* **104:** 556–565.

Murakami Y, Minami M, Daimon Y, Okanoue T. 2004. Hepatitis B virus DNA in liver, serum, and peripheral blood mononuclear cells after the clearance of serum hepatitis B virus surface antigen. *J Med Virol* **72:** 203–214.

Nakagawa H, Shibata T. 2013. Comprehensive genome sequencing of the liver cancer genome. *Cancer Lett* **340:** 234–240.

Oishi Y, Watanabe Y, Yoshida Y, Sato Y, Hiraishi T, Oikawa R, Maehata T, Suzuki H, Toyota M, Niwa H, et al. 2012. Hypermethylation of Sox17 gene is useful as a molecular diagnostic application in early gastric cancer. *Tumour Biol* **33:** 383–393.

Orend G, Kuhlmann I, Doerfler W. 1991. Spreading of DNA methylation across integrated foreign (adenovirus type 12) genomes in mammalian cells. *J Virol* **65:** 4301–4308.

Schriml LM, Padilla-Nash HM, Coleman A, Moen P, Nash WG, Menninger J, Jones G, Ried T, Dean M. 1999. Tyramide signal amplification (TSA)-FISH applied to mapping PCR-labeled probes less than 1 kb in size. *Biotechniques* **27:** 608–613.

Sells MA, Chen ML, Acs G. 1987. Production of hepatitis B virus particles in Hep G2 cells transfected with cloned hepatitis B virus DNA. *Proc Natl Acad Sci* **84:** 1005–1009.

Speel EJ, Ramaekers FC, Hopman AH. 1997. Sensitive multicolor fluorescence in situ hybridization using catalyzed reporter deposition (CARD) amplification. *J Histochem Cytochem* **45:** 1439–1446.

Sung WK, Zheng H, Li S, Chen R, Liu X, Li Y, Lee NP, Lee WH, Ariyaratne PN, Tennakoon C, et al. 2012. Genome-wide survey of recurrent HBV integration in hepatocellular carcinoma. *Nat Genet* **44:** 765–769.

Taniguchi Y, Nosaka K, Yasunaga J, Maeda M, Mueller N, Okayama A, Matsuoka M. 2005. Silencing of human T-cell leukemia virus type I gene transcription by epigenetic mechanisms. *Retrovirology* **2:** 64.

Tao Q, Robertson KD. 2003. Stealth technology: how Epstein-Barr virus utilizes DNA methylation to cloak itself from immune detection. *Clin Immunol* **109:** 53–63.

Toh ST, Jin Y, Liu L, Wang J, Babrzadeh F, Gharizadeh B, Ronaghi M, Toh HC, Chow PK, Chung AY, et al. 2013. Deep sequencing of the hepatitis B virus in hepatocellular carcinoma patients reveals enriched integration events, structural alterations and sequence variations. *Carcinogenesis* **34:** 787–798.

Toyota M, Ho C, Ahuja N, Jair KW, Li Q, Ohe-Toyota M, Baylin SB, Issa JP. 1999. Identification of differentially methylated sequences in colorectal cancer by methylated CpG island amplification. *Cancer Res* **59:** 2307–2312.

Uozaki H, Fukayama M. 2008. Epstein-Barr virus and gastric carcinoma-viral carcinogenesis through epigenetic mechanisms. *Int J Clin Exp Pathol* **1:** 198–216.

Watanabe Y, Castoro RJ, Kim HS, North B, Oikawa R, Hiraishi T, Ahmed SS, Chung W, Cho MY, Toyota M, et al. 2011. Frequent alteration of MLL3 frameshift mutations in microsatellite deficient colorectal cancer. *PLoS ONE* **6:** e23320.

Yamada Y, Ito T. 2011. Highly efficient PCR assay to discriminate allelic DNA methylation status using whole genome amplification. *BMC Res Notes* **4:** 179.

Received March 8, 2014; accepted in revised form December 29, 2014.

DNA methylation at hepatitis B viral integrants is associated with methylation at flanking human genomic sequences

Yoshiyuki Watanabe, Hiroyuki Yamamoto, Ritsuko Oikawa, et al.

Genome Res. published online February 4, 2015
Access the most recent version at doi:10.1101/gr.175240.114

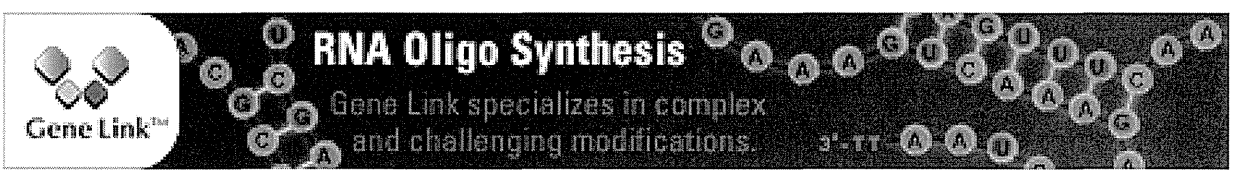

PLOS ONE

Antitumor Activity and Induction of TP53-Dependent Apoptosis toward Ovarian Clear Cell Adenocarcinoma by the Dual PI3K/mTOR Inhibitor DS-7423

Tomoko Kashiyama[1], Katsutoshi Oda[1]*, Yuji Ikeda[1], Yoshinobu Shiose[2], Yasuhide Hirota[2], Kanako Inaba[1], Chinami Makii[1], Reiko Kurikawa[1], Aki Miyasaka[1], Takahiro Koso[1], Tomohiko Fukuda[1], Michihiro Tanikawa[1], Keiko Shoji[1], Kenbun Sone[1], Takahide Arimoto[1], Osamu Wada-Hiraike[1], Kei Kawana[1], Shunsuke Nakagawa[3], Koichi Matsuda[4], Frank McCormick[5], Hiroyuki Aburatani[6], Tetsu Yano[7], Yutaka Osuga[1], Tomoyuki Fujii[1]

1 Department of Obstetrics and Gynecology, Faculty of Medicine, The University of Tokyo, Tokyo, Japan, **2** Oncology Research Laboratories, Daiichi Sankyo Co. Ltd., Tokyo, Japan, **3** Department of Obstetrics and Gynecology, Faculty of Medicine, Teikyo University, Tokyo, Japan, **4** Laboratory of Molecular Medicine, Human Genome Center, Institute of Medical Science, The University of Tokyo, Tokyo, Japan, **5** Helen Diller Family Comprehensive Cancer Center, University of California San Francisco, San Francisco, California, United States of America, **6** Genome Science Division, Research Center for Advanced Science and Technology, The University of Tokyo, Tokyo, Japan, **7** Department of Obstetrics and Gynecology, National Center for Global Health and Medicine, Tokyo, Japan

Abstract

DS-7423, a novel, small-molecule dual inhibitor of phosphatidylinositol-3-kinase (PI3K) and mammalian target of rapamycin (mTOR), is currently in phase I clinical trials for solid tumors. Although DS-7423 potently inhibits PI3Kα (IC_{50} = 15.6 nM) and mTOR (IC_{50} = 34.9 nM), it also inhibits other isoforms of class I PI3K (IC_{50} values: PI3Kβ = 1,143 nM; PI3Kγ = 249 nM; PI3Kδ = 262 nM). The PI3K/mTOR pathway is frequently activated in ovarian clear cell adenocarcinomas (OCCA) through various mutations that activate PI3K-AKT signaling. Here, we describe the anti-tumor effect of DS-7423 on a panel of nine OCCA cell lines. IC_{50} values for DS-7423 were <75 nM in all the lines, regardless of the mutational status of *PIK3CA*. In mouse xenograft models, DS-7423 suppressed the tumor growth of OCCA in a dose-dependent manner. Flow cytometry analysis revealed a decrease in S-phase cell populations in all the cell lines and an increase in sub-G1 cell populations following treatment with DS-7423 in six of the nine OCCA cell lines tested. DS-7423-mediated apoptosis was induced more effectively in the six cell lines without *TP53* mutations than in the three cell lines with *TP53* mutations. Concomitantly with the decreased phosphorylation level of MDM2 (mouse double minute 2 homolog), the level of phosphorylation of TP53 at Ser46 was increased by DS-7423 in the six cell lines with wild-type *TP53*, with induction of genes that mediate TP53-dependent apoptosis, including *p53AIP1* and *PUMA* at 39 nM or higher doses. Our data suggest that the dual PI3K/mTOR inhibitor DS-7423 may constitute a promising molecular targeted therapy for OCCA, and that its antitumor effect might be partly obtained by induction of TP53-dependent apoptosis in *TP53* wild-type OCCAs.

Citation: Kashiyama T, Oda K, Ikeda Y, Shiose Y, Hirota Y, et al. (2014) Antitumor Activity and Induction of TP53-Dependent Apoptosis toward Ovarian Clear Cell Adenocarcinoma by the Dual PI3K/mTOR Inhibitor DS-7423. PLoS ONE 9(2): e87220. doi:10.1371/journal.pone.0087220

Editor: Yuan-Soon Ho, Taipei Medical University, Taiwan

Received September 30, 2013; **Accepted** December 18, 2013; **Published** February 4, 2014

Funding: This work was supported by Daiichi Sankyo Co. Ltd., The Grant-in-Aid for Scientific Research (C), Grant Number 19599005 and 23592437 from the Ministry of Education, Culture, Sports, Science and Technology of Japan (to K Oda). This study was also performed as a research program of the Project for Development of Innovative Research on Cancer Therapeutics (P-Direct), Ministry of Education, Culture, Sports, Science and Technology of Japan (to T Yano). Yoshinobu Shiose and Yasuhide Hirota, employees of Daiichi Sankyo Co. Ltd, contributed to the experiments (in vivo experiments) as listed in the "contributions" of each author. The funders themselves had no role in study design, data collection and analysis, decision to publish, or preparation of the manuscript.

Competing Interests: Yoshinobu Shiose and Yasuhide Hirota are employees of Daiichi Sankyo Co. Ltd, which partly supported this work (to K Oda). DS-7423 is in clinical development by Daiichi Sankyo Co. Ltd and was provided by the company for use in this study. There are no other relevant COI related to employment, consultancy, patents, products in development, or marketed products. These COI do not alter the authors' adherence to all the PLOS ONE policies on sharing data and materials.

* E-mail: katsutoshi-tky@umin.ac.jp

Introduction

The phosphatidylinositol 3-kinase (PI3K)-AKT signaling pathway is frequently activated in various types of cancers, and several inhibitors that target this pathway have been developed as potential cancer therapeutics. The constitutive activation of the PI3K-AKT pathway results from various types of alterations, including the overexpression of receptor tyrosine kinases (RTKs), as well as mutations of *Ras*, the catalytic subunit p110α of phosphoinositide-3-kinase (*PIK3CA*), and *PTEN* [1]. Class I PI3Ks include four isoforms of the catalytic subunit (p110α, p110β, p110γ, and p110δ). Among these four isoforms, p110α is broadly mutated and predominantly activated in various types of human cancers, although p110β and p110δ might be selectively activated in certain tumors such as those with loss of PTEN function [2,3]. Mammalian target of rapamycin (mTOR) is the catalytic subunit found in two distinct complexes: the raptor-containing complex mTORC1 and the rictor-containing complex mTORC2 [4]. AKT activates mTORC1 signaling and also phosphorylates other downstream proteins, including GSK3β, forkhead box-O tran-

scription factors (FOXOs), and mouse double minute 2 homolog (MDM2) [5]. mTORC1 controls protein synthesis and cell proliferation via the phosphorylation of its downstream targets, 4E-BP1 and S6 kinase 1 (S6K1) [6]. Rapamycin and its analogs (rapalogs) block mTORC1 activity, but not mTORC2 activity [7]. One of the AKT downstream targets, MDM2, is a negative regulator of TP53 that induces its ubiquitination and subsequent degradation [8]. Although the cytostatic effects of PI3K pathway inhibitors have been reported in various types of cancers [9–12], targeting the PI3K pathway might induce cytotoxic effects by suppressing anti-apoptotic signals through the dephosphorylation of FOXOs and stabilization of TP53. It seems reasonable to suspect that targeting the PI3K-mTOR axis might be a promising therapeutic strategy to selectively induce apoptosis of cancer cells, especially those without mutations in *TP53*.

Epithelial ovarian cancer is a leading cause of death resulting from gynecological malignancies. Ovarian clear cell adenocarcinoma (OCCA) is the second most common cause of death from ovarian cancer, with a higher incidence in Asia, especially in Japan (>25%), than in other continents [13]. OCCA is derived primarily from ovarian endometriosis, and the clinical outcome is generally poor, owing to low response rates to conventional platinum-based chemotherapy [14]. Thus, novel therapeutic strategies are warranted to improve the clinical outcome of OCCA. In histological terms, ovarian serous adenocarcinoma (OSA) is the most common variant of ovarian carcinoma [15]. It is highly sensitive to platinum-based chemotherapy, with a primary clinical response rate of >70%. The mutational spectrum differs between OCCA and OSA, with *TP53* mutations observed in almost all (96%) OSA tumors, but in only 10% of OCCA tumors [15,16]. In particular, mutations of *RB1* and *BRCA1/2* are much more common in OSA than in OCCA. However, *PIK3CA* mutations are more frequent in OCCA (>40%) than in OSA (<10%) [17]. Although mutations of *KRAS* and *PTEN* are rare (<10%), the overexpression of several RTKs has been reported in OCCA, including human epidermal growth factor receptor 2 (HER2) with a frequency of approximately 40% and cMET with a frequency of approximately 30% [18–21]. Taken together, these observations suggest that the RTK-PI3K/mTOR signaling axis might be broadly activated in OCCA.

DS-7423 is a novel, small-molecule compound that inhibits both PI3K and mTOR (mTORC1/2). It inhibits all class I PI3K isoforms with greater potency against p110α than against the other p110 isoforms. Relevant activity (IC_{50} <200 nM) was not observed in any of the 227 kinases tested, except for Mixed Lineage Kinase 1 (MLK1) and Never-In-Mitosis Gene A (NIMA)-related kinase 2 (NEK2). The compound is currently in phase I clinical trials for solid tumors. In this study, we evaluated its anti-tumor efficacy in a panel of OCCA cell lines. We focused in particular on the ability of DS-7423 to induce apoptosis, and on whether the apoptosis might be mediated by TP53.

Materials and Methods

Small-molecule compounds

The small molecule compound DS-7423 was provided by the Daiichi-Sankyo Company, Ltd (Tokyo, Japan). The drug information about DS-7423 is available on the ClinicalTrials.gov website (NCT01364844). The mTOR inhibitor rapamycin was purchased from Cayman Chemical (Michigan, USA).

Cell lines

The OVTOKO, OVISE, OVMANA, RMG-I, OVSAHO, OVKATE, and OV1063 lines were purchased from the Japanese Collection of Research Bioresources (JCRB) Cell Bank (Osaka, Japan). The JHOC-7, JHOC-9, HTOA, JHOS-2, JHOS-3, and JHOS-4 cell lines were purchased from the RIKEN Cell Bank (Ibaraki, Japan). The TOV-21, ES-2, and SKOV3 cell lines were from the American Type Culture Collection (Manassas, VA). OVISE, OVTOKO, TOV-21G and ES2 were cultured in RPMI1640 medium containing 10% fetal bovine serum (FBS). OVMANA was cultured in RPMI medium containing 20% FBS, JHOC-7 in DMEM/F12 medium containing 10% FBS, JHOC-9 and RMG-I in DMEM/F12 medium containing 20% FBS, and SKOV3 in DMEM containing 10% FBS. The OVSAHO, OVKATE, OV1063, HTOA, JHOS-2, JHOS-3, and JHOS-4 lines were cultured in DMEM medium containing 10% FBS. The histological subtype of the SKOV3 cells was not unambiguously defined even after extensive analysis, although it was confidently identified as clear cell adenocarcinoma [22]. The immortalized epithelial cell line from an ovarian endometrial cyst was a generous gift from Dr. Satoru Kyo [23].

Polymerase chain reaction (PCR) and sequencing

The mutational status of all nine OCCA cell lines was analyzed by PCR and direct sequencing. The PCR conditions and primers for the analysis of *PTEN* (exons 1–9) and *K-Ras* (exon 1 and 2) sequences were described previously [24–26]. The entire coding region of *PIK3CA* was analyzed by reverse transcription (RT)-PCR with LA-Taq according to the manufacturer's protocol (Takara BIO, Madison, WI) [27]. The PCR primers for analysis of *TP53* (exons 4–8) were described previously [28].

Proliferation assays

Assays of the suppression of cell proliferation were performed with the Cell Counting Kit-8 using the tetrazolium salt WST-8 [2-(2-methoxy-4-nitrophenyl)-3-(4-nitrophenyl)-5-(2,4-disulfophenyl)-2H-tetrazolium, monosodium salt] (Dojindo, Tokyo, Japan) for the methyl thiazolyl tetrazolium (MTT) assay. Using 96-well plates, 2,000 cells were seeded on the appropriate medium and treated with increasing doses (0–2,500 nM) of DS-7423 or rapamycin for 72 h, starting from 24 h after seeding. Proliferation was quantified by monitoring the changes in the absorbance at 450 nm, which were normalized relative to the absorbance of cell cultures treated with DMSO alone.

Immunoblotting

Cells were treated with DS-7423 or rapamycin for the indicated time and at the indicated concentration, and were then lysed in the cell lysis buffer (Cell Signaling Technology, Beverly, MA). Antibodies to total Akt, phosphorylation of Akt (p-Akt) (Ser473, Thr308), p-GSK3beta (Ser9), total S6, p-S6 (Ser235/236, Ser 240/244), p-4EBP1 (Thr37/46), p-FOXO1 (Thr24), p-FOXO3a (Thr32), p-MDM2 (Ser 166), p-TP53 (Ser15), cleaved-PARP, and PARP (Cell Signaling Technology, Beverly, MA), beta-actin (Sigma-Aldrich, St. Louis, MO), TP53 (Santa Cruz, CA, USA) and p-TP53 (Ser46) (Calbiochem, Billerica, MA) were used for immunoblotting, as recommended by the manufacturers. Signals were detected using BioRAD western blotting systems (BioRAD, Hercules, CA) with the detection reagents ECL advance and ECL select (GE Healthcare, Piscataway, NJ).

Cell cycle analysis

Cells (5×10^5) were seeded in 60-mm dishes and treated with DS-7423 for 48 h. Floating and adherent cells were collected by trypsinization and washed twice with phosphate buffer saline (PBS). Cells were resuspended in cold 70% ethanol and

maintained at 4°C overnight. After being washed twice with PBS, cells were incubated in RNase A (0.25 mg/mL) (Sigma) for 30 min at 37°C, followed by staining with propidium iodide (PI; 50 μg/mL) (Sigma) at 4°C for 30 min in the dark. Cells were then analyzed using flow cytometry (BD FACS Calibur HG, Franklin Lakes, NJ). Cell cycle distribution was analyzed using CELL Quest pro ver. 3.1. (Beckman Coulter Epics XL, Brea, CA). All experiments were repeated three times.

Detection of apoptosis by staining with annexin-V FITC

Cells (5×10^5) were cultured in 60-mm plates for 24 h before treatment with either DMSO (control), and 156 nM DS-7423, or 2,500 nM DS-7423 for 48 h. Cells were trypsinized, washed twice with PBS, and then analyzed after double staining with annexin-V fluorescein isothiocyanate (FITC) (Abcam, Cambridge, MA) and PI. The apoptotic cell population was analyzed using flow cytometry. All experiments were performed three times.

Ethics statement for animal experiments

This study was approved by Animal Care and Use Committee, Daiichi-Sankyo Pharmaceutical Co. Ltd. Athymic mice were maintained in an SPF (Specific Pathogen Free) facility according to our institutional guidelines, and experiments were conducted under an approved animal protocol.

Tumor xenografts in nude mice

Specific pathogen-free female nude mice (BALB/cAJcl-nu/nu), 6 weeks old, were purchased from CLEA Japan, Inc (Tokyo, Japan). Subcutaneous xenograft tumors in the mice were established by the injection of a 100-μL suspension containing 5×10^6 cells of the TOV-21, RMG-I, or ES-2 lines in PBS. Tumors were removed after exponential growth, cut into 3-mm pieces, and transplanted subcutaneously into other mice for RMG-I cells. DS-7423 was suspended in 0.5 w/v% Methyl Cellulose 400 solution (Wako Pure Chemical Industries, Ltd.) Oral daily administration of DS-7423 started 8–22 days later, following the injection of the cells ($5–6\times10^6$ cells/0.1 mL). One week after tumor transplantation, mice were assigned randomly to one of the three treatment regimens: (1) non-treated control, (2) DS-7423 (1.5 mg/kg), (3) DS-7423 (3 mg/kg), and (4) DS-7423 (6 mg/kg). Each treatment group consisted of five mice. DS-7423 was injected orally (p.o.) once a day. Tumor volumes (in mm^3) were calculated by the formula: ([major axis] × [minor axis]^2/2). After the treatment, the tumors were removed and analyzed by western blotting. Tumor weight (wet weight) was measured, and the average weight was calculated for each group.

Semi-quantitative RT-PCR analysis

OCCA cells were treated with either DMSO or the indicated concentration of either DS-7423 or rapamycin for 24 h. Total RNAs of these cells were extracted with the RNeasy Mini Kit according to the manufacturer's instructions (QIAGEN, Valencia, CA). cDNAs were synthesized from total RNAs by using the Super Script III First-strand Synthesis SuperMix (Invitrogen, Carlsbad, CA). The exponential phase of the RT-PCR occurred between 15–30 cycles, and these cycles were monitored to allow semi-quantitative comparisons among the cDNAs developed from identical reactions. The primers and conditions for the amplification of *p53AIP1*, *p21,* and *GAPDH* sequences were described previously [29]. The PCR primers for *PUMA* were 5′-TGAGACAAGAGGAGCAGCAG-3′ (forward) and 5′-ACCTAATTGGGCTCCAT CTC-3′ (reverse). The primers for p53R2, TIGAR, GLS2, GADD45, 14-3-3 sigma and PAI-1 were described previously [30–35]. Each PCR regimen involved a 2-min initial denaturation step (94°C), which was followed by 15–30 cycles at 94°C for 30 s, then at 55°C for 30 s, and finally, at 72°C for 30 s using a Thermal Cycler Gene Atlas instrument (ASTEC, Fukuoka, Japan).

Gene silencing

Cells were plated at approximately 30% confluence in 100-mm plates and incubated for 24 h before transfection with small interfering RNA (siRNA) duplexes at the concentrations indicated, using Lipofectamine 2000 RNAiMAX (Invitrogen, Carlsbad, CA) and Opti-MEM medium (Life Technologies, Grand Island, NY). The siRNAs specific for TP53 were purchased from Invitrogen. A negative control kit was used as a control (Invitrogen, Carlsbad, CA).

Luciferase assay

Transfection was performed using Effectene reagent (QIAGEN, Valencia, CA) according to the manufacturer's recommendation. The TP53 expression plasmid (0.1 μg/μL) was cotransfected with pp53 TA Luc (0.25 μg/mL). The phRL CMV-Renilla plasmid (Promega, Madison, WI) was also transfected in all experiments as the internal control to normalize the transfection efficiency. The assays, each involving triplicate wells, were repeated three times.

Statistical analysis

The data were expressed as means ± standard deviations of three independent determinations. The significance of the difference between two samples was analyzed using the Student's t-test, and a p-value of <0.05 was considered to denote a statistically significant difference.

Results

Genetic alterations and activation of the PI3K-AKT signaling pathway in OCCA cell lines

We evaluated the phosphorylation (p-) levels of the proteins in the PI3K-AKT pathway by using an immortalized epithelial cell line from an ovarian endometrial cyst as a control. AKT was phosphorylated at Thr308 in seven of the nine OCCA cell lines tested (Figure 1). The cell lines OVMANA and ES-2 had low levels of p-AKT (Thr308) (Figure 1). The phosphorylation levels of S6, 4E-BP1 and/or FOXO1/3a, the downstream targets of AKT, were upregulated in the OCCA cells, including OVMANA and ES-2.

Four of the nine cell lines possessed *PIK3CA* mutations (44%) (Figure 1 and Table S1), and one of these four, TOV-21G, also possessed mutations in *PTEN* and *K-Ras* (11%). *TP53* mutations were detected in three cell lines (33%) (Table S1). The mutational status of *PIK3CA* was not associated with the phosphorylation of AKT or proteins that act downstream of AKT. Next, the expression and phosphorylation levels of three RTKs (HER2, HER3, and MET), which have been reported to be overexpressed in OCCA, were evaluated. The levels of phosphorylation of both HER2 (Tyr1221/1222) and HER3 (Tyr1289) were correlated with the abundances of these two proteins (Figure 1). p-HER2 and p-HER3 levels were elevated in four (44%: OVISE, SKOV3, JHOC7 and RMG-I) and six (67%: TOV-21G, OVISE, OVMANA, OVTOKO, JHOC-7 and RMG-I) cell lines, respectively (Figure 1). The expression of MET was higher in all nine OCCA cell lines than in the control, although the level of p-MET was increased in only two cell lines (22%: JHOC-7 and RMG-I). Taken together, all the OCCA cell lines, except for ES-2 and JHOC-9, possessed one or more activating alterations in the RTK-PI3K genes examined (Figure 1 and Table S1). Each of the

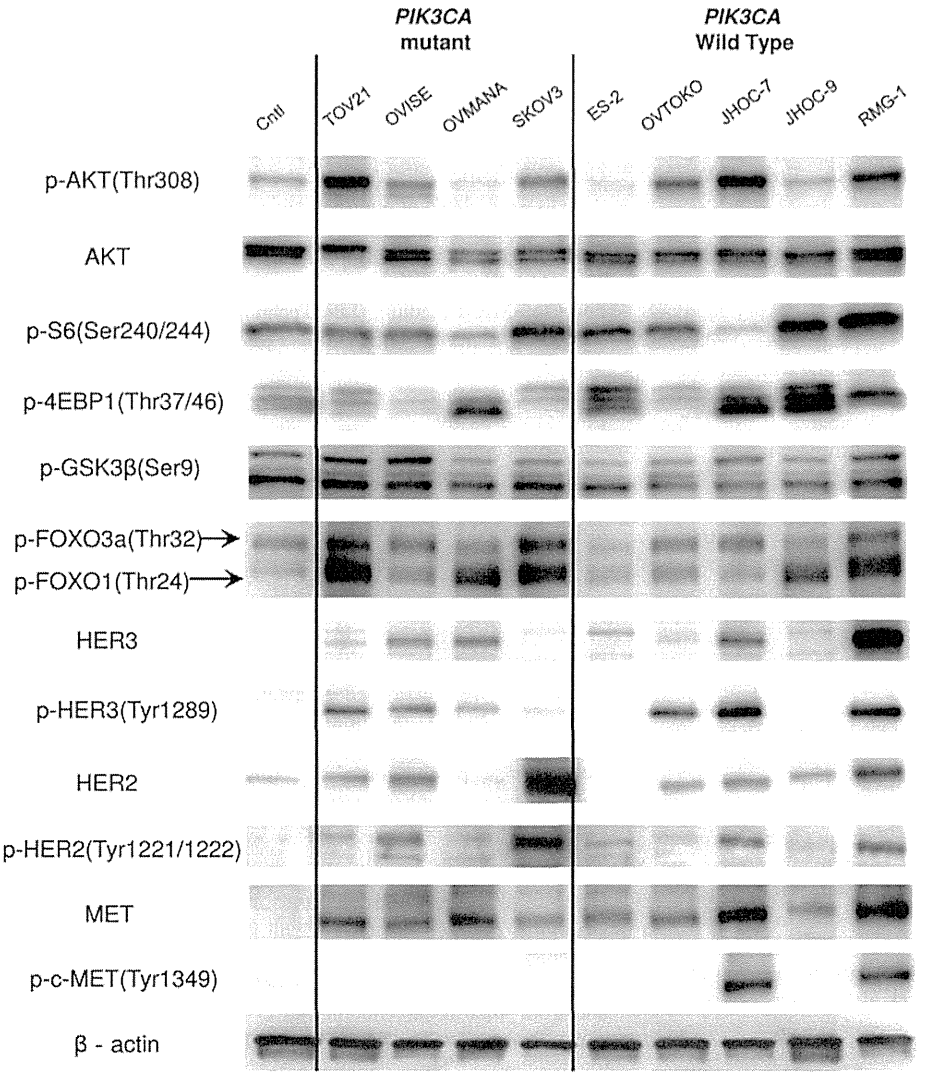

Figure 1. Phosphorylation and mutational status of genes that encode components of the RTK/Ras/PI3K pathway. Nine ovarian clear cell adenocarcinoma (OCCA) and a control (Cntl) cell line (immortalized epithelial cells from ovarian endometrioma) were lysed in cell lysis buffer and analyzed by western blotting. In general, most of the OCCA cell lines displayed higher levels of phosphorylation of Akt (Thr308) and its downstream targets (GSK3β, FOXO 1/3a, 4EBP1 and S6) than the respective levels of phosphorylation in the control line. The abundances and levels of phosphorylation of c-MET (Tyr1234/1235), HER2 (Tyr1221/1222), and HER3 (Tyr1289) were also evaluated. The mutational status of *PIK3CA*, *PTEN*, and *K-Ras* is shown for each cell line.
doi:10.1371/journal.pone.0087220.g001

four cell lines with *PIK3CA* mutations showed concomitant activation of RTKs, defined as high levels of phosphorylation of HER2 and/or HER3.

Anti-proliferative effect of DS-7423 in OCCA cell lines

We tested the anti-proliferative effects of the dual PI3K/mTOR inhibitor, DS-7423, and the mTOR (mTORC1) inhibitor, rapamycin, in each of the nine OCCA cell lines. Exposure to 156 nM DS-7423 inhibited cell growth by 70%–97%, and the IC_{50} values for cell proliferation were 20–75 nM (Figure 2A). Dose-dependent growth suppression was more clearly induced by DS-7423 than by rapamycin in each of the nine cell lines (Figure 2A). The IC_{50} value was not reached with rapamycin at any of the concentrations tested (2.45–2,560 nM) in five (OVMANA, SKOV3, OVTOKO, JHOC-7 and RMG-I) of the nine OCCA cell lines. We also examined the effect of DS-7423 in seven OSA lines. The IC_{50} values with DS-7423 were >100 nM in four of these seven OSAs (Figure 2B). The ratio of resistant cell lines (IC_{50} >100 nM) was significantly higher in OSA cell lines (57%) than in OCCA cell lines (0%) ($p = 0.019$ by Fisher's exact test).

We performed immunoblotting on the lysates prepared from the cells treated with DS-7423 or rapamycin. DS-7423 suppressed the phosphorylation of AKT (Thr308 and Ser473) and S6 (Ser235/236 and Ser240/244) at doses of 39–156 nM and higher (Figure 3A and Figure S1). DS-7423 suppressed the phosphorylation levels of the targeted proteins at comparable doses in the AKT pathway (AKT, FOXO1/3a, and MDM2) and mTORC1 pathway (S6). Rapamycin did not suppress p-Akt at any dose, and suppressed p-S6 at 2.45 nM or higher doses (Figure 3B). On the

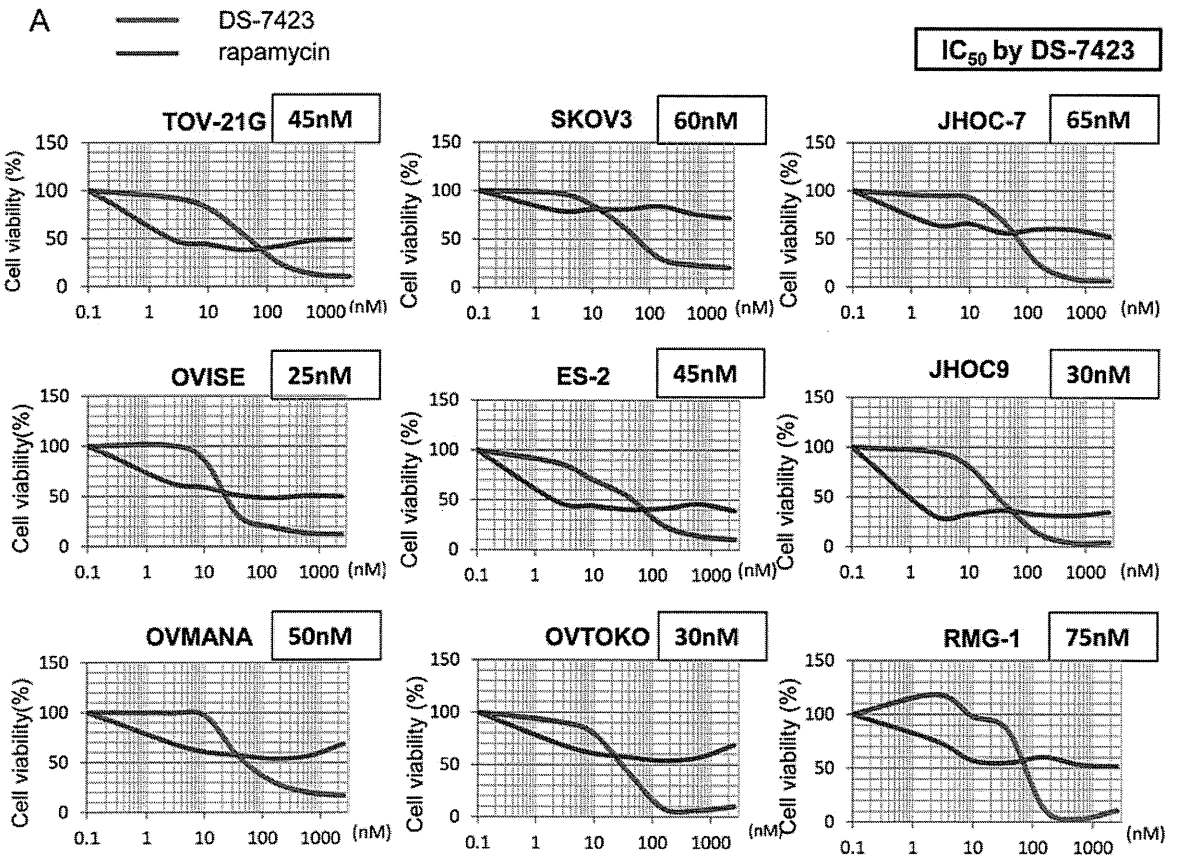

B

OSA	IC_{50} (nM)
JHOS-3	45
HTOA	60
OVSAHO	65
JHOS-4	120
JHOS-2	250
OV1063	700
OVKATE	>2,500

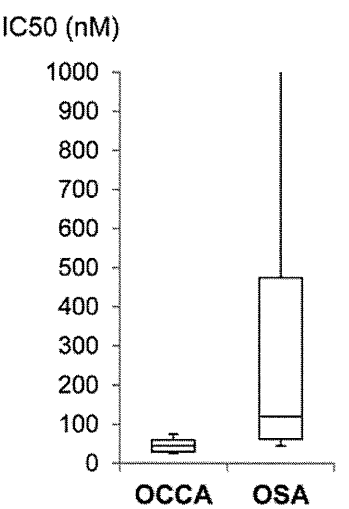

Figure 2. Inhibition of cell proliferation by DS-7423 and rapamycin. (A) Cell viability for each cell line was analyzed using the methyl thiazolyl tetrazolium (MTT) assay 72 h after treatment with DS-7423 or rapamycin at the doses indicated. The data were normalized relative to the value of the control cells. In all nine cell lines, DS-7423 suppressed cell proliferation more robustly than rapamycin when both were used at higher doses. (B) IC_{50} values for DS-7423 in seven ovarian serous adenocarcinoma (OSA) cell lines (left) were compared with those of nine OCCA cells (right). Four of seven OSA cells had IC_{50} values >100 nM, which is higher than that of any OCCA cells.
doi:10.1371/journal.pone.0087220.g002

contrary, rapamycin increased the levels of p-FOXO3a and p-FOXO1 at 2,500 nM (Figure 3B).

We conducted fluorescence-activated cell sorting (FACS)-based cell cycle analyses in OCCA cells treated with DS-7423. DS-7423 decreased the size of the S-phase population in the

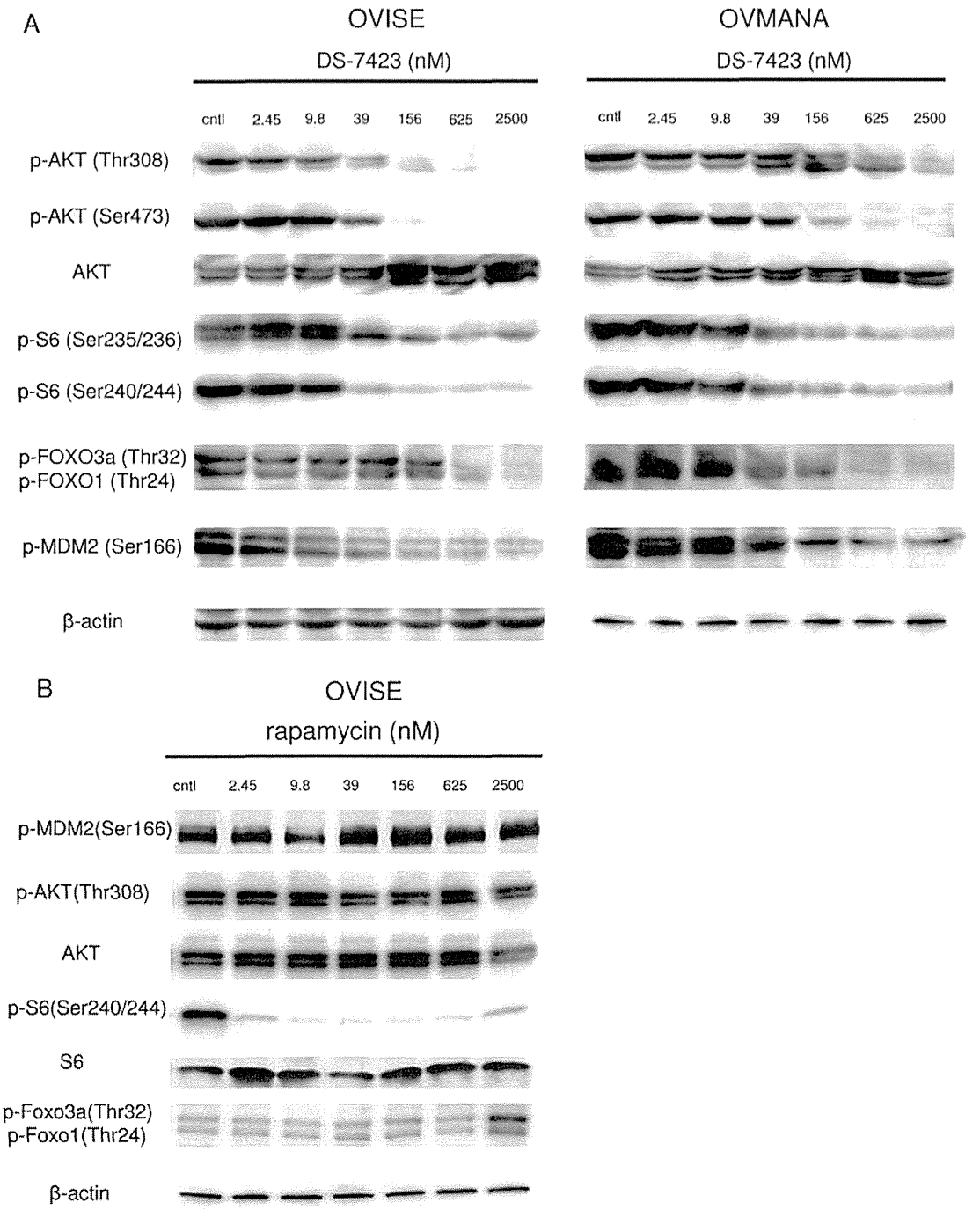

Figure 3. Inhibition of PI3K/mTOR signaling by DS-7423 and rapamycin in ovarian clear cell adenocarcinoma cell lines. (A) Immunoblotting of total protein extracts from OCCA cells (OVISE and OVMANA) treated with DS-7423 at concentrations ranging from 0 to 2,500 nM. (B) Immunoblotting of total protein extracts from OVISE cells treated with rapamycin at concentrations ranging from 0 to 2,500 nM.
doi:10.1371/journal.pone.0087220.g003

OCCA cells, although the change was weak in ES-2 cells. (Figure 4A). G1 arrest was predominantly observed in six of the nine cell lines. The sizes of sub-G1 populations increased in a dose-dependent manner in six of the nine cell lines, especially in OVISE and OVMANA cells.

In vivo antitumor effect of DS-7423 in a mouse xenograft model

In vivo antitumor activity of DS-7423 in mice implanted with either TOV-21G cells or RMG-1 tumor pieces was examined. Oral daily administration of DS-7423 significantly suppressed the tumor growth of the xenografts of TOV-21G and RMG-I in a

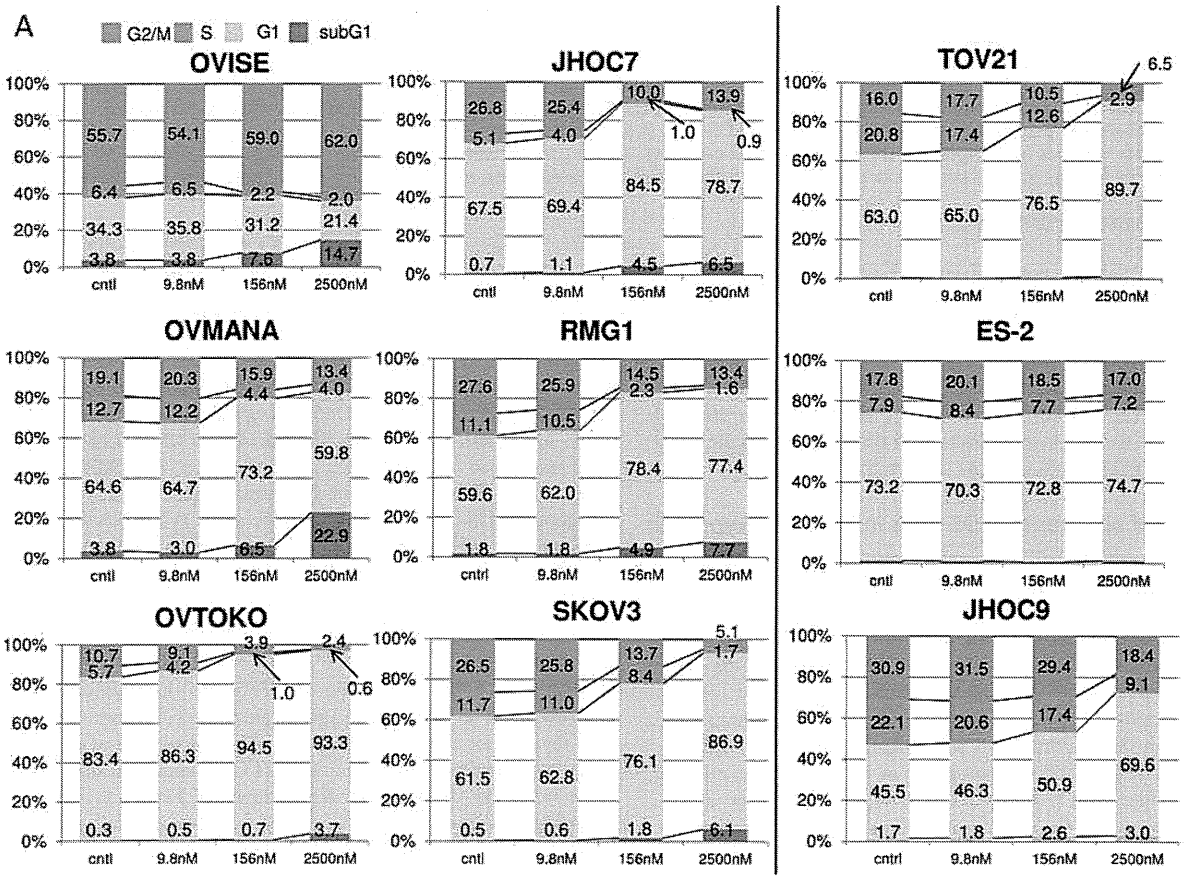
A
G2/M
S
G1
subG1
OVISE
JHOC7
TOV21
OVMANA
RMG1
ES-2
OVTOKO
SKOV3
JHOC9
100%
80%
60%
40%
20%
0%
cntl
9.8nM
156nM
2500nM
cntrl

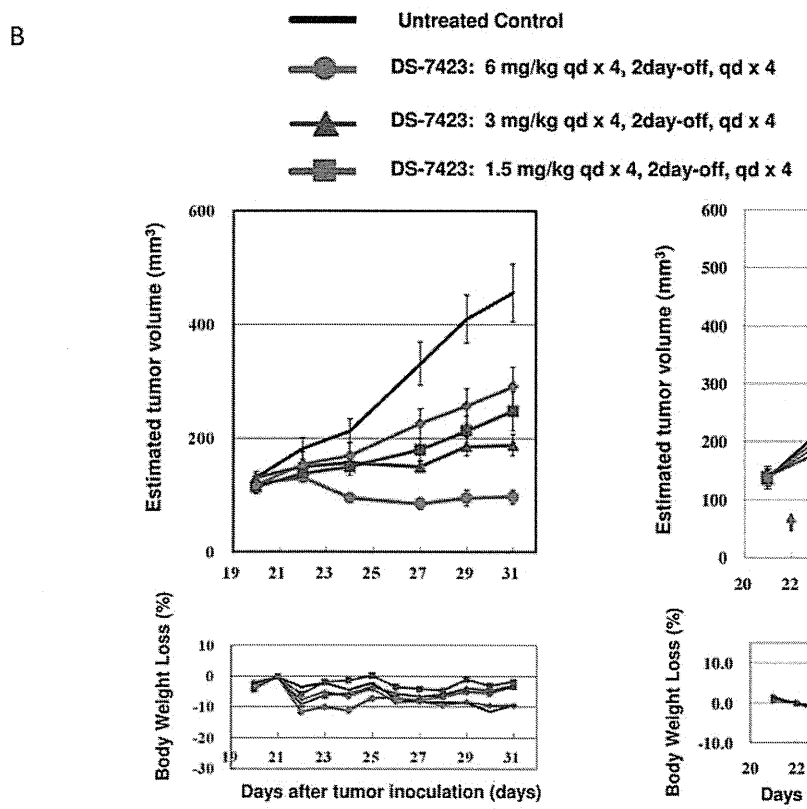
B
Untreated Control
DS-7423: 6 mg/kg qd x 4, 2day-off, qd x 4
DS-7423: 3 mg/kg qd x 4, 2day-off, qd x 4
DS-7423: 1.5 mg/kg qd x 4, 2day-off, qd x 4
Estimated tumor volume (mm3)
Body Weight Loss (%)
Days after tumor inoculation (days)

Figure 4. Flow cytometric analysis of the cell cycle in cancer cells treated with DS-7423, and *in vivo* demonstration of the anti-tumor effect of DS-7423 in nude mice. (A) Cells (5×10^5) were seeded in the presence of 10% serum and treated with DS-7423 for 48 h at doses of 9.8 nM, 256 nM, or 2,500 nM. DS-7423 blocked OCCA cell cycle progression into the S phase in a dose-dependent manner. The relative size of the sub-G1 population was increased in six of the cell lines (left) but was not affected in the remaining three cell lines (right). (B) Subcutaneous xenograft tumors in athymic BALB/c mice were established following the injection of OCCA cells of either the TOV-21G (left) or RMG-I (right) cell lines. Mice were treated daily (5–7 days per week) at the indicated doses of DS-7423 (1.5, 3, or 6 mg/kg, 8–10 days). Each treatment group contained five mice. Estimated tumor volumes (upper graphs) and body weight losses (BWL) (lower graphs) were shown in the two OCCA cells. Tumor volumes were calculated by the formula {(major axis)*(minor axis)^2/2} mm^3. Groups were compared at the end of treatment. Points, mean; bars, standard deviation (SD); *$p<0.05$.
doi:10.1371/journal.pone.0087220.g004

dose-dependent manner (Figure 4B). No significant adverse effects, including body weight loss of more than 10%, were observed in the mice examined (Figure 4B). Treatment with DS-7423 suppressed the levels of p-AKT (Thr308) and p-S6 (Ser240/244) in the TOV-21G and RMG-I xenografts (Figure S2A). Compared with TOV-21G and RMG-I xenografts, the anti-tumor effect of DS-7423 was weaker in xenografts with ES-2, for which the basal level of p-Akt (Thr-308) was low (Figure S2B).

Induction of apoptosis by DS-7423 in TP53 wild-type cell lines

The data collected from FACS analysis suggested that DS-7423 has a cytotoxic and cytostatic effect in certain OCCA cell lines. We combined the DS-7423 treatment (156 nM or 2,500 nM) with double staining with annexin-V FITC and PI to evaluate the proportion of cells that underwent apoptosis. DS-7423 at 156 nM induced apoptosis at 4–12% in five of the six cell lines that lacked mutations in *TP53* (Figure 5A and 5B). In these five cell lines, 2,500 nM DS-7423 induced apoptosis in 10–16% of the cells. In three cell lines with *TP53* mutations, DS-7423 did not induce apoptosis in >5% of the cells at any of the doses tested (Figure 5A). The size of the population of apoptotic cells was significantly higher in cells that lacked mutations in *TP3* when compared with cells with mutated *TP3* at either 156 nM ($p = 0.0352$) or 2,500 nM ($p = 0.0368$) DS-7423 according to the Student *t*-test (Figure 5C). Rapamycin did not induce apoptotic cell death in >5% of the OCCA cells, even at 2,500 nM. The percentage of apoptotic cells was significantly higher in OVISE cells treated with DS-7423 than that in those treated with rapamycin (Figure S3). This result indicates that mTORC1 inhibition alone is insufficient to induce apoptosis in OCCA cell lines. Immunoblotting analysis revealed that DS-7423 induced the cleavage of PARP within 2 h in OVMANA cells without mutations in *TP53* (Figure 5D). The induction of cleaved-PARP was observed at 39 nM, and the effect increased in a dose-dependent manner up to a concentration of 2,500 nM (Figure 5D).

Induction of p-TP53 at Ser46 and expression of *p53AIP1* by DS-7423

The phosphorylation of MDM2 is associated with the activation of MDM2 and degradation of TP53, with the phosphorylation of TP53 at Ser46 playing a key event in the TP53-dependent apoptosis (28). Treatment with DS-7423 reduced the level of p-MDM2 in a dose-dependent manner (Figure 3A and 6A). Inversely, DS-7423 increased TP53 level even at lower doses, resulting in increased expression of p-TP53 (Ser15 and Ser46) (Figure 6A). However, only p-TP53 (Ser46), not p-TP53 (Ser15), was clearly induced by high doses of DS-7423 (156–2,500 nM). We then used semi-quantitative RT-PCR to evaluate the regulation of genes that are directly regulated by TP53 in OVMANA and OVISE cells. DS-7423 induced the expression of the pro-apoptotic genes *p53AIP1* and *PUMA* at 39 nM or higher doses, but did not induce the expression of p21 at any of the three doses tested (39, 156, and 2,500 nM) (Figure. 6B and 6C). We also performed semi-quantitative RT-PCR of other TP53 target genes involved in DNA repair (p53R2), metabolism (TIGAR and GLS2), G2/M arrest (GADD45), and cell cycle arrest/senescence (14-3-3 sigma and PAI-1) to test whether other TP53 target genes are induced by DS-7423. GADD45 was significantly induced by DS-7423 in OVISE cells (Figure 6B and 6C), in which G2/M arrest was enhanced by DS-7423 according to the MTT assay (Figure 4A). The other TP53-downstream genes tested were not induced by DS-7423 in both OVISE and OVMANA cells, and expression of TIGAR was rather decreased in OVMANA cells (Figure S4).

TP53 activation is responsible for DS-7423-mediated apoptosis

We used siRNAs specific to *TP53* to knockdown *TP53* expression in OVISE cells, and treated the cells with DS-7423 at either 156 or 2,500 nM. The size of the population of apoptotic cells was calculated by annexin-V FITC–PI double staining 48 h after treatment of DS-7423. Knockdown of TP53 levels rescued cells from apoptotic cell death induced by treatment with both DS-7423 doses (Figure 6D). Immunoblotting indicated that two independent siRNAs (siRNA1 and siRNA2) specific to TP53 suppressed the expression of TP53 by >80% (Figure 6E). Next, we performed the MTT assay by applying both DS-7423 and siRNA to TP53 in OVISE cells (wild-type TP53). The anti-proliferative effect of DS-7423 was significantly reduced when combined with the knockdown of TP53 (Figure 6F). The effect of DS-7423 on the transcriptional activity of TP53 was also examined by luciferase assays in ES-2 cells with mutations in *TP53*. The cells were treated with DS-7423 for 24 h at the indicated doses, and then cotransfected with both pp53-TA-luc plasmid (containing TP53 binding sites) and a plasmid that encodes TP53. The relative luciferase activity of TP53 was significantly enhanced by DS-7423 in a dose-dependent manner (Figure 6G).

Discussion

The effects of the PI3K/mTOR inhibitor, DS-7423, on OCCA cell lines were examined with a particular focus on (i) the anti-proliferative effect of DS-7423, (ii) the induction of apoptosis by DS-7423, and (iii) the identification of predictive biomarkers for (i) and (ii).

MTT assays revealed a clear dose-dependent effect of DS-7423 on cell proliferation, with all nine OCCA cell lines displaying sensitivity to DS-7423 (IC_{50} at 75 nM or lower), regardless of mutations on *PIK3CA*. The sensitivity to DS-7423 was significantly higher in OCCA than in OSA cell lines. The prevalence in OCCA cell lines of activating mutations in genes that encode components of the RTK-PI3K-AKT signaling pathway might account, at least in part, for their broad sensitivity to DS-7423. Differences in the dose-dependence of the anti-proliferative effects of DS-7423 and rapamycin suggest differences in the modes of action of these two drugs. Whereas DS-7423 showed a more robust anti-proliferative

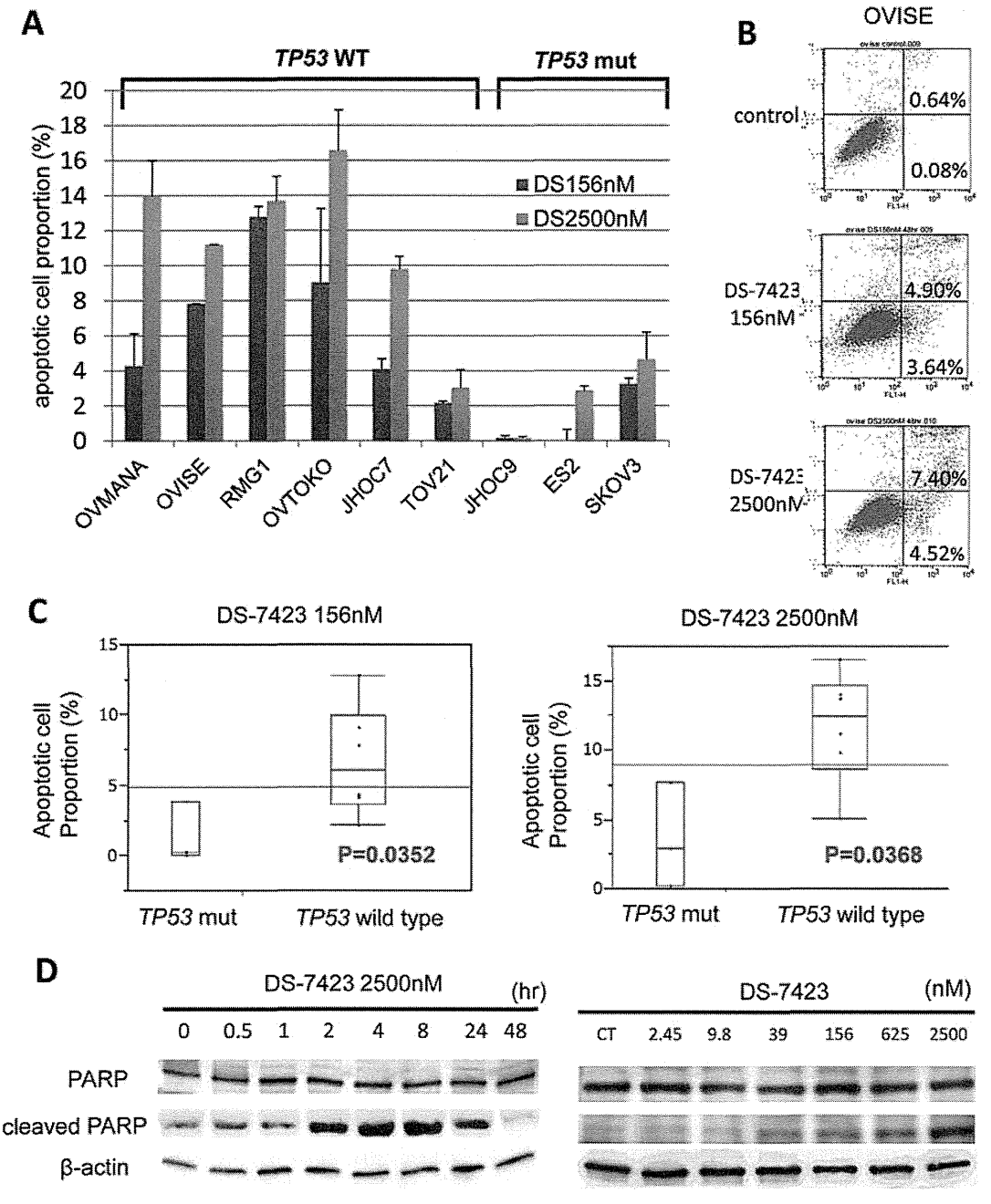

Figure 5. DS-7423-mediated induction of apoptosis in ovarian clear cell adenocarcinoma cell lines. (A) All nine OCCA cells were treated with DS-7423 at 156 or 2,560 nM for 48 h, and apoptotic cell proportion was evaluated using annexin-V fluorescein isothiocyanate (FITC) and propidium iodide (PI) double staining, followed by analysis using flow cytometry. The experiments were repeated 3 times, and each value is shown as the mean of 3 experiments ± standard deviation (SD). (B) The apoptotic cells were calculated using flow cytometry by counting the cell population in the right boxes. The example shown (OVISE cells) is representative of the results obtained for all the cell lines tested. (C) The proportion of cells rendered apoptotic by exposure to DS-7423 at 156 nM and 2,560 nM was significantly higher in OCCA cells without mutations in TP53 than in OCCA cells that carry mutations in TP53. (D) Cleaved poly(ADP-ribose) polymerase (PARP) induction was evaluated by immunoblotting in OVISE cells. OVISE cells were treated with DS-7423 at 156 nM for the times indicated (left) or for 4 h at the doses indicated (right).
doi:10.1371/journal.pone.0087220.g005

effect at the higher concentrations tested (>40 nM), rapamycin suppressed cell proliferation even at lower concentrations (<10 nM), and concentrations >10 nM failed to suppress the proliferation any further. This dose dependency is compatible with the phosphorylation levels of the target proteins in immunoblotting data and several previous reports in other types of cancers [10,12,36]. The cell cycle profile was distinct among each cell line. For example, G1 arrest was not induced and G2/M ratio was high in OVISE cells under DS-7423 exposure. This might be partly explained by the fact that GADD45 was induced by DS-7423 in

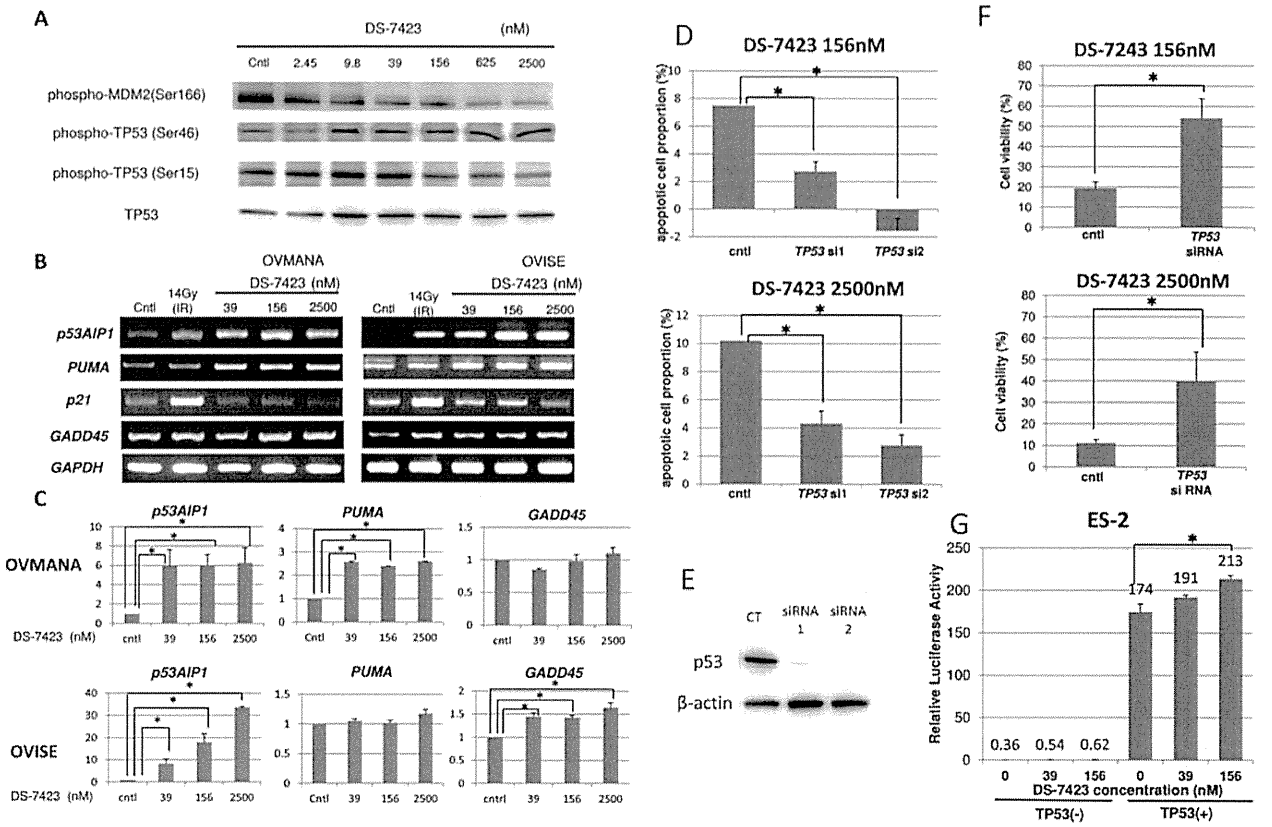

Figure 6. Induction of the phosphorylation of TP53 at Ser46 and the accumulation of transcripts of the genes targeted by TP53, which participate in TP53-mediated apoptosis. (A) Immunoblotting in OVMANA cells treated with DS-7423 at the indicated doses. Phosphorylation levels of MDM2 were inversely associated with p-TP53 at Ser46, but not with p-TP53 at Ser15. (B) Semi-quantitative RT-PCR in OVMANA and OVISE cells treated with DS-7423 at the indicated doses. Both *p53AIP1* and *PUMA* were induced by DS-7423. CT, untreated (negative) control; IR, irradiation at 14 Gy (positive control). GADD45 was induced in OVISE, but not in OVMANA cells. (C) Quantification of the semi-quantitative RT-PCR in (B). Each experiment was repeated 3 times, and each value is shown as the mean of 3 experiments ± SD. *p<0.05 (D) Effect of *TP53* knockdown on apoptosis induction by DS-7423. TP53 was knocked down by two independent siRNAs specific to *TP53* (siRNA1 and 2) in OVISE cells, which do not carry any mutation in *TP53*. The apoptotic cell population was evaluated using annexin-V staining, as described in Figure 5. The experiments were repeated 3 times, and each value is shown as the mean of 3 experiments ± SD. *p<0.05 (E) Suppression of TP53 expression by siRNAs was confirmed by immunoblotting. (F) Effect of *TP53* knockdown on cell proliferation by DS-7423 in MTT assay of OVISE cells. TP53 was knocked down by a siRNA1 specific to *TP53* and MTT assay was subsequently performed as in Figure 2. Knockdown of TP53 diminished the anti-proliferative effect caused by DS-7423 on OVISE cells. The experiments were repeated 3 times, and each value is shown as the mean of 3 experiments ± SD. *p<0.05 (G) TP53 expression plasmid (0.1 μg/μL) was cotransfected with pp53 TA Luc (0.25 μg/mL) plasmid into ES-2 cells mutated in *TP53*. The addition of DS-7423 increased the relative luciferase activity of TP53 in a dose-dependent manner. The experiments were repeated 3 times, and each value is shown as the mean of 3 experiments ± SD. *p<0.05.
doi:10.1371/journal.pone.0087220.g006

these cells. Thus, the action mechanism of DS-7423 might be distinct in each type of cells, regardless of the TP53 status. Resistance to mTOR (mTORC1) inhibitors might be induced by several mechanisms, including increased activity of another mTOR complex, mTORC2, or upregulation of receptor tyrosine kinases such as insulin-like growth factor-1 receptor (IGF-R1) [37,38]. The use of mTORC1 inhibitors to treat OCCAs is currently being investigated in phase 2 clinical trials. The currently ongoing GOG (Gynecologic Oncology Group)-0268 (NCT01196429) trial recruits OCCA patients and treats the subjects with carboplatin and paclitaxel, followed by temsirolimus (CCI-779). A report on six cases with weekly administration of temsirolimus in recurrent OCCA patients showed partial response in one patient and stable disease in another patient [39]. However, given that our data suggest that dual PI3K/mTOR inhibitors, such as DS-7423, might be more promising than single mTORC1 inhibitors, clinical trials that involve a dual PI3K/mTOR inhibitor, such as DS-7423, seem warranted for OCCA.

DS-7423 induced significantly higher levels of apoptotic cell death in OCCA cells without mutations in *TP53* than in OCCA cells with *TP53* mutations. This result suggests both that the mutational status of *TP53* might be a good biomarker to predict apoptosis induction by DS-7423, and that apoptosis depends on TP53 function. TP53 is degraded by MDM2, a ubiquitin ligase for TP53, and the MDM2 function is augmented by the kinase activity of Akt. Akt-mediated phosphorylation of MDM2 blocks its binding to p19ARF, increasing the degradation of TP53 [40,41]. DS-7423 increased the level of p-TP53 at Ser46, which results in induction of *p53AIP1* and *PUMA* (genes involved in TP53-mediated apoptosis) [29,42–44]. This data suggests that the apoptotic effect of DS-7423 depends, at least in part, on TP53 activity. The reasons for p-TP53 (Ser46), not p-TP53 (Ser15), being clearly induced and for apoptosis being preferentially

induced by high doses of DS-7423 should be further clarified. In addition, other non-apoptotic genes were not significantly induced by DS-7423, except for GADD45 in OVISE cells. Further analyses are warranted whether TP53 function is more involved in apoptosis rather than in cell cycle arrest and/or DNA repair process by DS-7423. Another possibility is that other proteins (such as FOXOs) which act downstream of Akt might also play a role in the induction [45]. Dephosphorylation of FOXOs at their Akt sites induces their nuclear translocation and triggers apoptosis by induction of prosurvival genes of the BCL2 family [46,47]. The observation that the phosphorylation of FOXO1/3a was suppressed by DS-7423, regardless of TP53 status, suggests that the pro-apoptotic effect of DS-7423 cannot be explained exclusively by the phosphorylation of FOXOs. The use of siRNA to knockdown TP53 rescued OCCA cells from apoptosis caused by DS-7423. We also confirmed by MTT assay that the anti-proliferative effect of DS-7423 was significantly diminished by knocking down TP53, suggesting that intact TP53 function might enhance the anti-tumor effect of DS-7423. Recently, it was reported that cell death caused by a PI3K inhibitor, BKM-120, was associated with TP53 status in glioma cells [48], and that PI3K/AKT inhibition was suggested to induce TP53-dependent apoptosis in HTLV-1-transformed cells [49]. These data also support the importance of wild-type TP53 in the induction of the cytotoxic effect of PI3K pathway inhibitors.

The involvement of multiple molecules in the activation of the PI3K/mTOR pathway underscores the critical need to develop predictive biomarkers that might also serve as therapeutic targets. Mutations of *PIK3CA* and amplification of *HER2* have been proposed to be useful biomarkers in breast cancer [50,51], whereas mutant Ras has been suggested to be a biomarker of resistance in several solid tumor cells [52]. All these biomarkers (*PIK3CA*, HER2 and Ras) are focused on the RTK/Ras/PI3K pathway itself, and not on the cytotoxic effects associated with PI3K/mTOR inhibitors. Our data suggest that the presence of *PIK3CA* mutation and any other PI3K-activating alteration alone might not predict the sensitivity of OCCA cells to DS-7423. ES-2 cells, with no mutations in the RTK/Ras/PI3K pathway genes examined, showed low level of p-Akt, and the effect of DS-7423 in ES-2 xenografts was less robust, suggesting that the level of PI3K pathway activation would still be important for the sensitivity. However, the mutational status of TP53 might represent a better biomarker for the selection of tumors that could be killed by DS-7423 treatment. The frequency of mutations in *TP53* in OCCA was much less frequent than for ovarian cancers with other histology types [15,53]. These results indicate that OCCAs would be good candidates for clinical studies on the dual PI3K/mTOR inhibitor, DS-7423.

Our study has several limitations. First, cytostatic effect is still essential to suppress cell proliferation, regardless of TP53 status. Second, the ratio of apoptotic cells is low (less than 20%) even at high concentrations of DS-7423. Third, the mechanism of cytostatic effect by DS-7423 in OCCA is cell type dependent (i.e. G1 arrest was not induced in OVISE and ES-2 cells). Thus, careful consideration is required to evaluate the TP53-dependent cytotoxic effect of DS-7423. Further studies are warranted to elucidate the mechanism of action of DS-7423, and more efficient induction of apoptosis might be needed for clinical application of this drug in OCCA.

Supporting Information

Figure S1 Immunoblotting of OCCA cells (ES-2 and JHOC-9), treated with DS-7423 at concentrations ranging from 0 to 2,500 nmol/L. As shown in Figure 3, phosphorylation of AKT and its target proteins were downregulated by DS-7423. In ES-2 cells, basal level of p-AKT at Thr 308 was very low (as shown in Fig. 1), but p-AKT at Ser473 was clearly suppressed by DS-7423.
(PPTX)

Figure S2 *In vivo* effect of DS-7423 in nude mice. (A) Western blot of total lysates from the TOV-21G and RMG-1 xenografts. total lysates were harvested 2 and 6 h after the last drug administration of DS-7423. The levels of p-Akt (Thr-308) and p-S6 (Ser-240/244) were assessed. (B) Subcutaneous xenograft tumors in athymic BALB/c mice were established after injection of ES-2 cells. Mice were treated daily at the indicated doses (1.5, 3 or 6 mg/kg/day, totally 8 times) of DS-7423 or non-treated control. Estimated tumor volumes were smaller in mice treated daily with 6 mg/kg of DS-7423, compared to the control. Western blot of total lysates from the ES-2 xenografts (treated with 6 mg/kg of DS-7423) was also shown below.
(PPTX)

Figure S3 The size of apoptotic cell population was compared between DS-7423 and rapamycin in OVISE cells, using annexin-V FITC and PI double staining (as shown in Fig. 5A–5B). The percentage of apoptotic cells was significantly higher in cells treated with DS-7423, compared with those with rapamycin.
(PPTX)

Figure S4 Semi-quantitative RT-PCR in OVMANA and OVISE cells treated with DS-7423 at the indicated doses. Each expression level of p53R2, TIGAR, GLS2, GADD45, 14-3-3 sigma and PAI-1 was not enhanced by DS-7423. Each experiment was repeated 3 times, and each value is shown as the mean of 3 experiments ± SD.
(PPTX)

Table S1 Phosphorylation and mutational status in 9 OCCA cell lines. Elevated phosphorylation of cMET, HER2 and HER3, and mutations of *PIK3CA*, *PTEN*, *KRAS* and *TP53* were listed in each cell line.
(XLSX)

Acknowledgments

We thank Satoru Kyo for the generous gift of the immortalized cell line.

Author Contributions

Conceived and designed the experiments: T Kashiyama KO YS YH KM. Performed the experiments: T Kashiyama YI YS YH KI CM RK. Analyzed the data: T Kashiyama KO YS YH. Contributed reagents/materials/analysis tools: YI AM T Koso T Fukuda MT K Shoji K Sone TA OW-H KK SN KM FM HA TY YO T Fujii. Wrote the paper: T Kashiyama KO.

References

1. Yuan TL, Cantley LC (2008) PI3K pathway alterations in cancer: variations on a theme. Oncogene 27: 5497–510.
2. Jia S, Liu Z, Zhang S, Liu P, Zhang L, et al. (2008) Essential roles of PI(3)K-p110beta in cell growth, metabolism and tumorigenesis. Nature 454: 776–9.
3. Wee S, Wiederschain D, Maira SM, Loo A, Miller C, et al. (2008) PTEN-deficient cancers depend on PIK3CB. Proc Natl Acad Sci USA 105: 13057–13062.
4. Zoncu R, Efeyan A, Sabatini DM (2011) mTOR: from growth signal integration to cancer, diabetes and ageing. Nat Rev Mol Cell Biol 12: 21–35.

5. Engelman JA (2009) Targeting PI3K signalling in cancer: opportunities, challenges and limitations. Nat Rev Cancer 9: 550–562.
6. Sabatini DM (2006) mTOR and cancer: insights into a complex relationship. Nat Rev Cancer 6: 729–734.
7. Guertin DA, Sabatini DM (2007) Defining the role of mTOR in cancer. Cancer Cell 12: 9–22.
8. Mayo LD, Donner DB (2001) A phosphatidylinositol 3-kinase/Akt pathway promotes translocation of Mdm2 from the cytoplasm to the nucleus. Proc Natl Acad Sci USA 98: 11598–11603.
9. Maira SM, Stauffer F, Brueggen J, Furet P, Schnell C, et al. (2008) Identification and characterization of NVP-BEZ235, a new orally available dual phosphatidylinositol 3-kinase/mammalian target of rapamycin inhibitor with potent in vivo antitumor activity. Mol Cancer Ther 7: 1851–1863.
10. Serra V, Markman B, Scaltriti M, Eichhorn PJ, Valero V, et al. (2008) NVP-BEZ235, a dual PI3K/mTOR inhibitor, prevents PI3K signaling and inhibits the growth of cancer cells with activating PI3K mutations. Cancer Res 68: 8022–8030.
11. Cao P, Maira SM, Garcia Echeverria C, Hedley DW (2009) Activity of a novel, dual PI3-kinase/mTor inhibitor NVP-BEZ235 against primary human pancreatic cancers grown as orthotopic xenografts. Br J Cancer 100: 1267–1276.
12. Shoji K, Oda K, Kashiyama T, Ikeda Y, Nakagawa S, et al. (2012) Genotype-dependent efficacy of a dual PI3K/mTOR inhibitor, NVP-BEZ235, and an mTOR inhibitor, RAD001, in endometrial carcinomas. PLoS One 7: e37431.
13. Anglesio MS, Carey MS, Kobel M, Mackay H, Huntsman DG (2011) Clear cell carcinoma of the ovary: A report from the first Ovarian Clear Cell Symposium, June 24th, Gynecol Oncol 2010. 121: 407–415.
14. Takano M, Tsuda H, Sugiyama T (2012) Clear cell carcinoma of the ovary: is there a role of histology-specific treatment? J Exp Clin Cancer Res 31: 53–59.
15. Bell D, Berchuck A, Birrer M, Chien J, Cramer D, et al. (2011) Integrated genomic analyses of ovarian carcinoma. Nature 474: 609–615. Cancer Genome Atlas Research Network.
16. Ho ES, Lai CR, Hsieh YT, Chen JT, Lin AJ, et al. (2001) p53 mutation is infrequent in clear cell carcinoma of the ovary. Gynecol Oncol 80: 189–193.
17. Kuo KT, Mao TL, Jones S, Veras E, Ayhan A, et al. (2009) Frequent activating mutations of PIK3CA in ovarian clear cell carcinoma. Am J Pathol 174: 1597–1601.
18. Munksgaard PS, Blaakaer J (2012) The association between endometriosis and ovarian cancer: a review of histological, genetic and molecular alterations. Gynecol Oncol 124: 164–169.
19. Fujimura M, Katsumata N, Tsuda H, Uchi N, Miyazaki S, et al. (2002) HER2 is frequently over-expressed in ovarian clear cell adenocarcinoma: possible novel treatment modality using recombinant monoclonal antibody against HER2, trastuzumab. Jpn J Cancer Res 93: 1250–1257.
20. Yamamoto S, Tsuda H, Miyai K, Takano M, Tamai S, et al. (2011) Gene amplification and protein overexpression of MET are common events in ovarian clear-cell adenocarcinoma: their roles in tumor progression and prognostication of the patient. Mod Pathol 24: 1146–1155.
21. Yamamoto S, Tsuda H, Miyai K, Takano M, Tamai S, et al. (2012) Accumulative copy number increase of MET drives tumor development and histological progression in a subset of ovarian clear-cell adenocarcinomas. Mod Pathol 25: 122–130.
22. Shaw TJ, Senterman MK, Dawson K, Crane CA, Vanderhyden BC (2004) Characterization of intraperitoneal, orthotopic, and metastatic xenograft models of human ovarian cancer. Mol Ther 10: 1032–1042.
23. Bono Y, Kyo S, Takakura M, Maida Y, Mizumoto Y, et al. (2012) Creation of immortalised epithelial cells from ovarian endometrioma. Br J Cancer 106: 1205–1213.
24. Minaguchi T, Yoshikawa H, Oda K, Ishino T, Yasugi T, et al. (2001) PTEN mutation located only outside exons 5, 6, and 7 is an independent predictor of favorable survival in endometrial carcinomas. Clin Cancer Res 7: 2636–2642.
25. Samuels Y, Wang Z, Bardelli A, Silliman N, Ptak J, et al. (2004) High frequency of mutations of the PIK3CA gene in human cancers. Science 304: 554.
26. Oda K, Stokoe D, Taketani Y, McCormick F (2005) High frequency of coexistent mutations of PIK3CA and PTEN genes in endometrial carcinoma. Cancer Res 65: 10669–10673.
27. Oda K, Okada J, Timmerman L, Rodriguez Viciana P, Stokoe D, et al. (2008) PIK3CA cooperates with other phosphatidylinositol 3′-kinase pathway mutations to effect oncogenic transformation. Cancer Res 68: 8127–8136.
28. Nakagawa S, Yoshikawa H, Jimbo H, Onda T, Yasugi T, et al. (1999) Elderly Japanese women with cervical carcinoma show higher proportions of both intermediate-risk human papillomavirus types and p53 mutations. Br J Cancer 79: 1139–1144.
29. Oda K, Arakawa H, Tanaka T, Matsuda K, Tanikawa C, et al. (2000) p53AIP1, a potential mediator of p53-dependent apoptosis, and its regulation by Ser-46-phosphorylated p53. Cell 102: 849–862.
30. Hermeking H, Lengauer C, Polyak K, He TC, Zhang L, et al (1997) 14-3-3 sigma is a p53-regulated inhibitor of G2/M progression. Mol Cell 1: 3–11.
31. Zhan Q, Antinore MJ, Wang XW, Carrier F, Smith ML, et al (1999) Association with Cdc2 and inhibition of Cdc2/Cyclin B1 kinase activity by the p53-regulated protein Gadd45. Oncogene 18: 2892–2900.
32. Tanaka H, Arakawa H, Yamaguchi T, Shiraishi K, Fukuda S, et al (2000) A ribonucleotide reductase gene involved in a p53-dependent cell-cycle checkpoint for DNA damage. Nature 404: 42–49.
33. Kortlever RM, Higgins PJ, Bernards R (2006) Plasminogen activator inhibitor-1 is a critical downstream target of p53 in the induction of replicative senescence. Nat Cell Biol 8: 877–884.
34. Bensaad K, Tsuruta A, Selak MA, Vidal MN, Nakano K, et al (2006) TIGAR, a p53-inducible regulator of glycolysis and apoptosis. Cell 126: 107–120.
35. Suzuki S, Tanaka T, Poyurovsky MV, Nagano H, Mayama T, et al (2010) Phosphate-activated glutaminase (GLS2), a p53-inducible regulator of glutamine metabolism and reactive oxygen species. Proc Natl Acad Sci U S A 107: 7461–7466.
36. Cho DC, Cohen MB, Panka DJ, Collins M, Ghebremichael M, et al. (2010) The efficacy of the novel dual PI3-kinase/mTOR inhibitor NVP-BEZ235 compared with rapamycin in renal cell carcinoma. Clin Cancer Res 16: 3628–3638.
37. O'Reilly KE, Rojo F, She QB, Solit D, Mills GB, et al. (2006) mTOR inhibition induces upstream receptor tyrosine kinase signaling and activates Akt. Cancer Res 66: 1500–1508.
38. Wan X, Harkavy B, Shen N, Grohar P, Helman LJ (2007) Rapamycin induces feedback activation of Akt signaling through an IGF-1R-dependent mechanism. Oncogene 26: 1932–1940.
39. Takano M, Kikuchi Y, Kudoh K, Goto T, Furuya K, et al. (2011) Weekly administration of temsirolimus for heavily pretreated patients with clear cell carcinoma of the ovary: a report of six cases. Int J Clin Oncol 16: 605–609.
40. Haupt Y, Maya R, Kazaz A, Oren M (1997) Mdm2 promotes the rapid degradation of p53. Nature 387: 296–299.
41. Ogawara Y, Kishishita S, Obata T, Isazawa Y, Suzuki T, et al. (2002) Akt enhances Mdm2-mediated ubiquitination and degradation of p53. J Biol Chem 277: 21843–21850.
42. Nakano K, Vousden KH (2001) PUMA, a novel proapoptotic gene, is induced by p53. Mol Cell 7: 683–694.
43. Matsuda K, Yoshida K, Taya Y, Nakamura K, Nakamura Y, et al. (2002) p53AIP1 regulates the mitochondrial apoptotic pathway. Cancer Res 62: 2883–2889.
44. Vousden KH, Prives C (2009) Blinded by the Light: The Growing Complexity of p53. Cell 137: 413–421.
45. Fu Z, Tindall DJ (2008) FOXOs, cancer and regulation of apoptosis. Oncogene 27: 2312–2319.
46. Rahmani M, Anderson A, Habibi JR, Crabtree TR, Mayo M, et al. (2009) The BH3-only protein Bim plays a critical role in leukemia cell death triggered by concomitant inhibition of the PI3K/Akt and MEK/ERK1/2 pathways. Blood 114: 4507–4516.
47. Letai A (2006) Growth factor withdrawal and apoptosis: the middle game. Mol Cell 21: 728–730.
48. Koul D, Fu J, Shen R, LaFortune TA, Wang S, et al (2012) Antitumor activity of NVP-BKM120– a selective pan class I PI3 kinase inhibitor showed differential forms of cell death based on p53 status of glioma cells. Clin Cancer Res 18: 184–195.
49. Jeong SJ, Dasgupta A, Jung KJ, Um JH, Burke A, et al (2008) PI3K/AKT inhibition induces caspase-dependent apoptosis in HTLV-1-transformed cells. Virology 370: 264–272.
50. She QB, Chandarlapaty S, Ye Q, Lobo J, Haskell KM, et al. (2008) Breast tumor cells with PI3K mutation or HER2 amplification are selectively addicted to Akt signaling. PLoS One 3: e3065.
51. O'Brien C, Wallin JJ, Sampath D, GuhaThakurta D, Savage H, et al. (2010) Predictive biomarkers of sensitivity to the phosphatidylinositol 3′ kinase inhibitor GDC-0941 in breast cancer preclinical models. Clin Cancer Res 16: 3670–3683.
52. Ihle NT, Lemos R Jr, Wipf P, Yacoub A, Mitchell C, et al. (2009) Mutations in the phosphatidylinositol-3-kinase pathway predict for antitumor activity of the inhibitor PX-866 whereas oncogenic Ras is a dominant predictor for resistance. Cancer Res 69: 143–150.
53. Petitjean A, Achatz MI, Borresen Dale AL, Hainaut P, et al. (2005) TP53 mutations in human cancers: functional selection and impact on cancer prognosis and outcomes. Oncogene 26: 2157–2165.

Downregulation of the tumor suppressor HSPB7, involved in the p53 pathway, in renal cell carcinoma by hypermethylation

JIAYING LIN[1,2], ZHENZHONG DENG[1], CHIZU TANIKAWA[1], TARO SHUIN[3], TSUNEHARU MIKI[4], KOICHI MATSUDA[1] and YUSUKE NAKAMURA[1,2]

[1]Laboratory of Molecular Medicine, Human Genome Center, Institute of Medical Science, University of Tokyo, Tokyo 108-8639, Japan; [2]Section of Hematology/Oncology, Department of Medicine, University of Chicago, Chicago, IL 60637, USA; [3]Department of Urology, School of Medicine, Kochi University, Kochi 783-8505; [4]Department of Urology, Kyoto Prefectural University of Medicine, Kyoto 602-8566, Japan

Received December 10, 2013; Accepted January 27, 2014

DOI: 10.3892/ijo.2014.2314

Abstract. In order to identify genes involved in renal carcinogenesis, we analyzed the expression profile of renal cell carcinomas (RCCs) using microarrays consisting of 27,648 cDNA or ESTs, and found a small heat shock protein, HSPB7, to be significantly and commonly downregulated in RCC. Subsequent quantitative PCR (qPCR) and immunohistochemical (IHC) analyses confirmed the downregulation of HSPB7 in RCC tissues and cancer cell lines in both transcriptional and protein levels. Bisulfite sequencing of a genomic region of HSPB7 detected DNA hypermethylation of some segments of HSPB7 in RCC cells and concordantly 5-aza-2'-deoxycytidine (5-Aza-dC) treatment of cancer cells restored HSPB7 expression significantly. Ectopic introduction of HSPB7 in five RCC cell lines remarkably suppressed cancer cell growth. Interestingly, we found that HSPB7 expression could be induced by p53 in a dose-dependent manner, indicating that this gene functions in the p53 pathway. Our results imply that HSBP7 is likely to be a tumor suppressor gene regulated by p53 and its downregulation by hypermethylation may play a critical role in renal carcinogenesis.

Introduction

Renal cell carcinoma (RCC) accounts for approximately 2% of all cancers worldwide (1) and its incidence has increased by 2-3% in the last decade with even higher rate in developed countries (2-6). The underlying mechanisms such as some environmental and genetic risk factors including smoking, obesity, acquired cystic kidney disease and inherited susceptibility (von Hippel-Lindau disease) (3,7,8) have been indicated, but the etiological and pathological mechanisms of this disease are still far from fully understood.

Although local renal tumors can be surgically removed (9-11), distant metastasis is often observed even if the primary tumor is relatively small (12,13). Patients with metastatic RCC generally result in extremely poor outcomes with overall median survival of around 13 months and the 5 year survival rate of <10% (13). For the advanced-stage patients, systemic therapy including immunotherapy (e.g. IL-2, IFN-α) and/or molecular-targeted drugs (e.g. sunitinib, bevacizumab, sorafenib, temsirolimus and everolimus) is recommended (14), but the response rates are not satisfactory.

To better understand the molecular mechanisms of renal carcinogenesis and apply the information for the development of effective treatment and early diagnosis, we performed genome-wide gene expression profile analysis and identified a small heat shock protein, HSPB7, whose function in cancer is unknown, to be downregulated in a great majority of human RCC samples.

In this study, we attempted to address two key questions, i) whether HSPB7 has growth suppressive function and ii) how HSPB7 is downregulated in RCCs. We here report for the first time that HSPB7 is likely to be a tumor suppressor which is frequently downregulated by DNA methylation in RCCs and is involved in the p53 pathway.

Materials and methods

Tissue samples and cell lines. Tissue samples used in this study were obtained from patients with written informed consent at three hospitals: Juntendo University School of Medicine, Kochi University School of Medicine, and Kyoto Prefectural University of Medicine. The human RCC cell lines (Caki-1, Caki-2, 786-O, A-498, ACHN), HEK293 and NCI-H1299 (lung carcinoma, p53-null) were purchased from American Type Culture Collection (ATCC; Rockville, MD, USA). Colon cancer cell lines HCT116 p53 wild-type ($p53^{+/+}$) and its derivative ($p53^{-/-}$) were gifts from Dr B. Vogelstein

Correspondence to: Professor Yusuke Nakamura, Section of Hematology/Oncology, Department of Medicine and Surgery, University of Chicago, Knapp Center for Biomedical Discovery, Room 6130, 900 E 57th St., Chicago, IL 60637, USA
E-mail: ynakamura@bsd.uchicago.edu

Key words: HSPB7, renal cell carcinoma, hypermethylation, p53

(Johns-Hopkins University, Baltimore, MD, USA). Normal human renal proximal tubule epithelial cells (RPTEC) were purchased from Lonza Walkersville Inc. (Walkersville, MD, USA). All cell lines were grown in monolayers in appropriate media recommended by suppliers: Dulbecco's modified Eagle's medium (Gibco, Carlsbad, CA, USA) for HEK293, HCT116 ($p53^{-/-}$) and HCT116 ($p53^{+/+}$); Eagle's minimal essential medium (Gibco) for A-498; McCoy's 5A medium (Gibco) for Caki-1 and Caki-2; RPMI-1640 medium (Gibco) for ACHN, 786-O and NCT-H1299; in addition, cells were supplemented with 10% fetal bovine serum (Cell Culture Bioscience, Nichirei Biosciences, Inc., Tokyo, Japan) except ACHN (5%), and 1% penicillin-streptomycin-amphotericin B suspension (Wako, Osaka, Japan). RPTEC were grown in REGM™ BulletKit, purchased from Lonza Walkersville Inc. (Walkersville, MD, USA). All cells were maintained at 37˚C in humid air with 5% CO_2 condition. Cells were transfected with plasmids using FuGENE 6 transfection reagent (Roche, Basel, Switzerland) or Lipofectamine LTX and Plus reagent (Invitrogen, Carlsbad, CA, USA) according to the manufacturer's protocols.

cDNA microarray and selection of candidate genes. We prepared a genome-wide cDNA microarray with totally 27,648 cDNAs/ESTs selected from the UniGene database of the National Center for Biotechnology Information (NCBI). This microarray system was constructed as previously described (15,16). We analyzed 15 clear cell renal cell carcinomas (RCC) and selected candidate genes according to the following criteria: i) genes for which we were able to obtain expression data in more than 50% of the cancers examined; ii) genes whose expression ratio was <0.2 in more than 50% of informative cases; and iii) the function of the gene was still unknown. Through these criteria, several candidates including HSPB7 were further validated. Gene expression data were deposited in the Gene Expression Omnibus database (accession no. GSE39364).

Quantitative real-time PCR (qPCR). We extracted total RNA from the microdissected RCC clinical samples, microdissected normal renal cortex, 25 different normal organs (17) and cultured cells using RNeasy mini kits (Qiagen, Valencia, CA, USA). RNAs from cell lines were reversely transcribed using the oligo (dT)21 primer and SuperScript III reverse transcriptase (Invitrogen). RNAs from tissue samples were treated with DNase I and subjected to two rounds of RNA amplification using T7-based *in vitro* transcription (Epicentre Technologies, Madison, WI, USA), then amplified RNAs were reversely transcribed to single-stranded cDNAs using random primer with Superscript II reverse transcriptase (Invitrogen) according to the manufacturer's instruction. qPCR was conducted using the SYBR-Green I Master (Roche) on a LightCycler 480 (Roche). Standard curve method was used for quantification analysis, and β2 microglobulin (B2M) served as a control gene. The qPCR primers for HSPB7 in cell lines were: 5'-ACTTCTCACCTGAAGA CATCATTG-3' (forward) and 5'-CATGACAGTGCCG TCAGC-3' (reverse). The qPCR primers for HSPB7 in tissues were: 5'-GACCTTCCATCAGCCTTAACC-3' (forward) and 5'-ATGTGGGAGACGAAACCAAG-3' (reverse). The qPCR process was started at 95˚C for 5 min, then underwent 45 cycles at 95˚C for 10 sec, 55˚C for 10 sec and 72˚C for 10 sec. Data analysis including standard curve generation and copy number calculation was performed automatically. Each reaction was performed in duplicate and negative controls were included in each experiment.

Immunohistochemistry (IHC). A kidney tissue array (BioChain Institute, Inc., USA) was used to analyze the protein expression of HSPB7 by IHC staining. This tissue array included 11 cases of RCC with corresponding normal tissues from the same patients as controls. Tissue sections were deparaffinized, rehydrated, and processed under high pressure (125˚C, 30 sec) in antigen-retrieval solution of pH 9.0 (S2367, Dako, Carpinteria, CA, USA). Sections were blocked with Protein Block Serum Free (Dako) for 1 h at room temperature, followed by incubation with primary antibody (HSPB7, 1:100, Proteintech, Chicago, IL, USA) overnight at 4˚C. At day 2, endogenous peroxidase activity was blocked by incubation in 3% hydrogen peroxide for 30 min at room temperature. Sections were incubated with a secondary antibody (Dako Envision$^+$ system-HRP labeled polymer anti-rabbit K4003) for 30 min at room temperature, followed by DAB staining (K3468, Dako), counter stained with hematoxylin QS (H-3404, Vector Laboratories, Burlingame, CA, USA), dehydrated and mounted. Three independent investigators semi-quantitatively assessed the HSPB7 positivity without prior knowledge of clinicopathological data. According to the intensity of HSPB7 staining, these samples were evaluated as: negative (-), weakly positive (+), moderate positive (++), and strong positive (+++). HSPB7 negative or weakly positive (-/+) were considered low expression, and moderate or strong positive were considered high expression (++/+++).

5-Aza-2'-deoxycytidine (5-Aza-dC) treatment. 5-Aza-dC (Sigma-Aldrich, St. Louis, MO, USA) was dissolved in DMSO. For a negative control, 5 RCC cell lines were treated with DMSO alone for 4 days. For a 5-Aza-dC group, cells were treated with DMSO for 1 day, following 5-Aza-dC-treatment (1, 3 and 10 μM, respectively) for 3 days. On the fifth day, total RNAs of all cells were isolated using the RNeasy mini kits (Qiagen, Valencia, CA, USA), according to the manufacturer's directions. qPCR was subsequently performed to detect the expression of HSPB7. To detect the protein level of HSPB7 in 5 RCC cell lines after the same treatment (5-Aza-dC 1 μM was used in 5-Aza-dC group), western blot and immunocytochemical (ICC) analyses were performed.

Bisulfite sequencing. Genomic DNA was extracted from RPTEC, HEK293 and 5 RCC cell lines (Caki-1, Caki-2, 786-O, A-498, ACHN) using the DNeasy blood and tissue kit (Qiagen). Genomic DNA (3.5 μg each) were digested at 37˚C for 16 h with 35 units of *Xho*I (Takara, Tokyo, Japan) and 1X H buffer (Takara) in 50 μl of reaction volume. After treatment with phenol/chloroform/isoamyl alcohol (25:24:1, v/v), the DNA was finally dissolved in TE buffer and denatured in 0.3 N NaOH for 20 min at 37˚C, and then the unmethylated cytosine residues were sulfonated by incubation in 3.12 M of sodium bisulfite (pH 5.0, Sigma-Aldrich) and 0.5 mM of hydroquinone (Sigma-Aldrich) at 55˚C for 16 h. The sulfonated DNA was recovered using the